Published for SISSA by Springer

Received: *April 6, 2011*
Revised: *October 16, 2011*
Accepted: *November 8, 2011*
Published: *November 24, 2011*

New physics in $b \to s\mu^+\mu^-$: CP-conserving observables

Ashutosh Kumar Alok,[a] **Alakabha Datta,**[b] **Amol Dighe,**[c] **Murugeswaran Duraisamy,**[b] **Diptimoy Ghosh**[c] **and David London**[a]

[a] *Physique des Particules, Université de Montréal, C.P. 6128, succ. centre-ville, Montréal, QC - H3C 3J7, Canada*
[b] *Department of Physics and Astronomy, University of Mississippi, 108 Lewis Hall, Oxford, MS 38677-1848, U.S.A.*
[c] *Tata Institute of Fundamental Research, Homi Bhabha Road, Mumbai 400005, India*

E-mail: alok@lps.umontreal.ca, datta@phy.olemiss.edu, amol@theory.tifr.res.in, duraism@phy.olemiss.edu, diptimoyghosh@theory.tifr.res.in, london@lps.umontreal.ca

Abstract: We perform a comprehensive study of the impact of new-physics operators with different Lorentz structures on decays involving the $b \to s\mu^+\mu^-$ transition. We examine the effects of new vector-axial vector (VA), scalar-pseudoscalar (SP) "‘ and tensor (T) interactions on the differential branching ratios and forward-backward asymmetries (A_{FB}'s) of $\bar{B}_s^0 \to \mu^+\mu^-$, $\bar{B}_d^0 \to X_s\mu^+\mu^-$, $\bar{B}_s^0 \to \mu^+\mu^-\gamma$, $\bar{B}_d^0 \to \bar{K}\mu^+\mu^-$, and $\bar{B}_d^0 \to \bar{K}^*\mu^+\mu^-$, taking the new-physics couplings to be real. In $\bar{B}_d^0 \to \bar{K}^*\mu^+\mu^-$, we further explore the polarization fraction f_L, the angular asymmetry $A_T^{(2)}$, and the longitudinal-transverse asymmetry A_{LT}. We identify the Lorentz structures that would significantly impact these observables, providing analytical arguments in terms of the contributions from the individual operators and their interference terms. In particular, we show that while the new VA operators can significantly enhance most of the asymmetries beyond the Standard Model predictions, the SP and T operators can do this only for A_{FB} in $\bar{B}_d^0 \to \bar{K}\mu^+\mu^-$.

Keywords: Beyond Standard Model, B-Physics

ArXiv ePrint: 1008.2367

© SISSA 2011

doi:10.1007/JHEP11(2011)121

JHEP11(2011)121

Contents

JHEP11(2011)121

1 Introduction

In recent years, there have been quite a few measurements of quantities in B decays which differ from the predictions of the Standard Model (SM) by $\sim 2\sigma$. For example, in $B \to \pi K$, the SM has some difficulty in accounting for all the experimental measurements [1]. The measured indirect (mixing-induced) CP asymmetry in some $b \to s$ penguin decays is found not to be identical to that in $B^0_d \to J/\psi K_S$ [2–4], counter to the expectations of the SM. While the SM predicts that the indirect CP asymmetry in $\bar{B}^0_s \to J/\psi\phi$ should be $\simeq 0$, the measurement of this quantity by the CDF and DØ collaborations shows a deviation from the SM [5]. One naively expects the ratio of transverse and longitudinal polarizations of the decay products in $B \to \phi K^*$ to be $f_T/f_L \ll 1$, but it is observed that $f_T/f_L \simeq 1$ [6, 7]. It may be possible to explain this value of f_T/f_L within the SM, but this is not certain. Finally, the recent observation of the anomalous dimuon charge asymmetry by the DØ collaboration [8] also points towards some new physics in B_s mixing that affects the lifetime difference and mixing phase involved therein (for example, see ref. [9]). Though none of the measurements above show a strong enough deviation from the SM to claim positive evidence for new physics (NP), they are intriguing since (i) the effects are seen in several different B decay channels, (ii) use a number of independent observables, and (iii) all involve $b \to s$ transitions.

A further hint has recently been seen in the leptonic decay channel: in the exclusive decay $\bar{B}^0_d \to \bar{K}^*\mu^+\mu^-$, the forward-backward asymmetry (A_{FB}) has been found to deviate somewhat from the predictions of the SM [10, 11, 13, 14]. This is interesting since it is a CP-conserving process, whereas most of the other effects involve CP violation. Motivated by this tantalizing hint of NP in $\bar{B}^0_d \to \bar{K}^*\mu^+\mu^-$, we explore the consequences of such NP in related decays. We do not restrict ourselves to any particular model, but work in the framework of effective operators with different Lorentz structures.

If NP affects $\bar{B}^0_d \to \bar{K}^*\mu^+\mu^-$, it must be present in the decay $b \to s\mu^+\mu^-$, and will affect the related decays $\bar{B}^0_s \to \mu^+\mu^-$, $\bar{B}^0_d \to X_s\mu^+\mu^-$, $\bar{B}^0_s \to \mu^+\mu^-\gamma$, and $\bar{B}^0_d \to \bar{K}\mu^+\mu^-$. The analyses of these decays in the context of the SM as well as in some NP models have been performed in the literature: $\bar{B}^0_s \to \mu^+\mu^-$ [15–25], $\bar{B}^0_d \to X_s\mu^+\mu^-$ [26–35], $\bar{B}^0_s \to \mu^+\mu^-\gamma$ [36–44], $\bar{B}^0_d \to \bar{K}\mu^+\mu^-$ [32, 45–51], $\bar{B}^0_d \to \bar{K}^*\mu^+\mu^-$ [52–67]. Correlations between some of these modes have been studied in refs. [68–70].

In this paper, we consider the addition of NP vector-axial vector (VA), scalar-pseudoscalar (SP), and tensor (T) operators that contribute to $b \to s\mu^+\mu^-$, and compute their effects on the above decays. Our aim here is not to obtain precise predictions, but rather to obtain an understanding of how the NP affects the observables, and to establish which Lorentz structure(s) can provide large deviations from the SM predictions. Some of these effects have already been examined by some of us: for example, new VA and SP operators in $\bar{B}^0_s \to \mu^+\mu^-$ [21], new VA and SP operators in $\bar{B}^0_s \to \mu^+\mu^-\gamma$ [43], the correlation between $\bar{B}^0_s \to \mu^+\mu^-$ and $\bar{B}^0_d \to \bar{K}\mu^+\mu^-$ with SP operators [69, 70], large forward-backward asymmetry in $\bar{B}^0_d \to \bar{K}\mu^+\mu^-$ from T operators [49], and the contribution of all Lorentz structures to $\bar{B}^0_d \to \bar{K}^*\mu^+\mu^-$, with a possible explanation of the A_{FB} anomaly [62]. Here we perform a combined study of all of these decay modes with all the

JHEP11(2011)121

Lorentz structures, consolidating and updating some of the earlier conclusions, and adding many new results and insights. Such a combined analysis, performed here for the first time, is crucial for obtaining a consistent picture of the bounds on NP and the possible effect of NP on the observables of interest. While observables like the differential branching ratio (DBR) and $A_{FB}(q^2)$ by themselves are sensitive to NP, we also examine the correlations between them in the context of NP Lorentz structures.

A full angular distribution of $\bar{B}_d^0 \to \bar{K}^* \mu^+ \mu^-$ allows us access to many independent observables, and hence to multiple avenues for probing NP. We present here for the first time the full angular distribution, including all the NP Lorentz structures, for this decay mode. This leads to the identification of observables that could be significantly influenced by specific Lorentz structures of NP. In addition to the DBR and A_{FB}, we also examine the longitudinal polarization fraction f_L and the angular asymmetry $A_T^{(2)}$, introduced recently in ref. [57]. We further analyze the longitudinal-transverse asymmetry A_{LT}, which, as we will argue, has very small hadronic uncertainties.

Hadronic uncertainties often are the main source of error in the calculation of SM predictions of a quantity, and make the positive identification of NP rather difficult. In this paper, for $\bar{B}_d^0 \to \bar{K} \mu^+ \mu^-$ we use the form factors from light-cone sum rules. For $\bar{B}_d^0 \to \bar{K}^* \mu^+ \mu^-$, we use the form factors obtained from QCD factorization at low q^2, and those from light-cone sum rules at high q^2. The latest next-to-leading order (NLO QCD) corrections [71] have not been included. These corrections would affect the central values of the SM predictions to a small extent, while also decreasing the renormalization-scale uncertainty. However, since our primary interest is looking for observables for which the NP effects are large, a LO analysis is sufficient at this stage. In our figures, we display bands for the SM predictions that include the form-factor uncertainties as claimed by the respective authors.

In addition to the form-factor uncertainties, the SM prediction bands also include the uncertainties due to quark masses, Cabibbo-Kobayashi-Maskawa (CKM) matrix elements and meson decay constants. In our figures, these bands are overlaid with some examples of the allowed values of these observables when NP contributions are included. This allows the scaling of these uncertainties to be easily visualized. It turns out that in many cases, the results with the NP can be significantly different from those without the NP, even taking into account inflated values for the hadronic uncertainties. We identify and emphasize such observables. We also show that the hadronic uncertainties in several of these observables are under control, especially when the invariant mass of the muon pair is small and one can use the limit of large-energy effective theory (LEET). This makes such observables excellent probes of new physics. Also, since all the observables are shown as functions of q^2, we have the information not just about the magnitudes of the observables, but also about their shape as a function of q^2, where some of the uncertainties are expected to cancel out.

In this paper, we restrict ourselves to real values for all the NP couplings, and study only the CP-conserving observables.[1] In section 2, we examine the various SM and NP

[1]The CP-violating observables, with complex values of the couplings, are treated in the companion paper [72].

JHEP11(2011)121

$b \to s\mu^+\mu^-$ operators, and give the current constraints on the NP couplings. The effects of the NP operators on the observables of the decays are discussed in the following sections: $\bar{B}_s^0 \to \mu^+\mu^-$ (section 3), $\bar{B}_d^0 \to X_s\mu^+\mu^-$ (section 4), $\bar{B}_s^0 \to \mu^+\mu^-\gamma$ (section 5), $\bar{B}_d^0 \to \bar{K}\mu^+\mu^-$ (section 6), and $\bar{B}_d^0 \to \bar{K}^*\mu^+\mu^-$ (section 7). Our notation in these sections clearly distinguishes the contributions from VA, SP and T operators and their interference terms, which offers many insights into their impact on modifying the observables. We give the details of the calculations involved in sections 4–7 in the appendices A–D, respectively, for the sake of completeness and in order to have a clear consistent notation for this combined analysis. In section 8, we summarize our findings and discuss their implications. In particular, we point out the measurements which will allow one to distinguish among the different classes of NP operators, and thus clearly identify which type of new physics is present.

2 $b \to s\mu^+\mu^-$ operators

2.1 Standard Model and new physics: effective Hamiltonians

Within the SM, the effective Hamiltonian for the quark-level transition $b \to s\mu^+\mu^-$ is

$$\begin{aligned}\mathcal{H}_{\rm eff}^{\rm SM} = -\frac{4G_F}{\sqrt{2}}V_{ts}^*V_{tb}\Bigg\{\sum_{i=1}^{6}C_i(\mu)\mathcal{O}_i(\mu) + C_7\,\frac{e}{16\pi^2}\,[\bar{s}\sigma_{\mu\nu}(m_sP_L + m_bP_R)b]\,F^{\mu\nu} \\ + C_9\,\frac{\alpha_{em}}{4\pi}\,(\bar{s}\gamma^\mu P_L b)\,\bar{\mu}\gamma_\mu\mu + C_{10}\,\frac{\alpha_{em}}{4\pi}\,(\bar{s}\gamma^\mu P_L b)\,\bar{\mu}\gamma_\mu\gamma_5\mu\Bigg\}\,,\end{aligned} \tag{2.1}$$

where $P_{L,R} = (1 \mp \gamma_5)/2$. The operators $\mathcal{O}_i$ $(i = 1, \ldots 6)$ correspond to the P_i in ref. [31], and $m_b = m_b(\mu)$ is the running b-quark mass in the $\overline{\rm MS}$ scheme. We use the SM Wilson coefficients as given in ref. [61]. In the magnetic dipole operator with the coefficient C_7, we neglect the term proportional to m_s.

The operators O_i, i = 1-6, can contribute indirectly to $b \to s\mu^+\mu^-$ and their effects can be included in an effective Wilson coeficient as [61]

$$\begin{aligned}C_9^{\rm eff} = C_9(m_b) + h(z,\hat{m}_c)\left(\frac{4}{3}C_1 + C_2 + 6\,C_3 + 60\,C_5\right) \\ - \frac{1}{2}h(z,\hat{m}_b)\left(7C_3 + \frac{4}{3}C_4 + 76C_5 + \frac{64}{3}C_6\right) \\ - \frac{1}{2}h(z,0)\left(C_3 + \frac{4}{3}C_4 + 16\,C_5 + \frac{64}{3}C_6\right) + \frac{4}{3}C_3 + \frac{64}{9}C_5 + \frac{64}{27}C_6\,.\end{aligned} \tag{2.2}$$

Here $z \equiv q^2/m_b^2$, and $\hat{m}_q \equiv m_q/m_b$ for all quarks q. The function $h(z,\hat{m})$ represents the one-loop correction to the four-quark operators O_1-O_6 and is given by [27, 61]

$$\begin{aligned}h(z,\hat{m}) = -\frac{8}{9}\ln\frac{m_b}{\mu_b} - \frac{8}{9}\ln\hat{m} + \frac{8}{27} + \frac{4}{9}x \\ -\frac{2}{9}(2+x)|1-x|^{1/2}\begin{cases}\left(\ln\left|\frac{\sqrt{1-x}+1}{\sqrt{1-x}-1}\right| - i\pi\right), & \text{for } x \le 1\,,\\ 2\arctan\frac{1}{\sqrt{x-1}}, & \text{for } x > 1\,,\end{cases}\end{aligned} \tag{2.3}$$

JHEP11(2011)121

where $x \equiv 4\hat{m}^2/z$. In the numerical analysis, the renormalization scale μ_b is varied between $m_b/2$ and $2m_b$. Note that in the high-q^2 region one can perform an operator product expansion (OPE) in $1/Q$ with $Q = (m_b\sqrt{q^2})$ [73, 74]. Numerically the results of refs. [73, 74] differ little from those in eq. (2.2) and so we use the above expression for the entire range of q^2. An analysis of $b \to s\mu^+\mu^-$ where the OPE in the high-q^2 region is used can be found in refs. [64, 66].

We now add new physics to the effective Hamiltonian for $b \to s\mu^+\mu^-$, so that it becomes

$$\mathcal{H}_{\rm eff}(b \to s\mu^+\mu^-) = \mathcal{H}_{\rm eff}^{\rm SM} + \mathcal{H}_{\rm eff}^{VA} + \mathcal{H}_{\rm eff}^{SP} + \mathcal{H}_{\rm eff}^{T}\,, \tag{2.4}$$

where $\mathcal{H}_{\rm eff}^{\rm SM}$ is given by eq. (2.1), while

$$\begin{aligned}
\mathcal{H}_{\rm eff}^{VA} &= -\frac{4G_F}{\sqrt{2}}\frac{\alpha_{em}}{4\pi}V_{ts}^*V_{tb}\Big\{R_V\,(\bar{s}\gamma^\mu P_L b)\,\bar{\mu}\gamma_\mu\mu + R_A\,(\bar{s}\gamma^\mu P_L b)\,\bar{\mu}\gamma_\mu\gamma_5\mu \\
&\qquad + R'_V\,(\bar{s}\gamma^\mu P_R b)\,\bar{\mu}\gamma_\mu\mu + R'_A\,(\bar{s}\gamma^\mu P_R b)\,\bar{\mu}\gamma_\mu\gamma_5\mu\Big\}\,, \qquad (2.5)\\
\mathcal{H}_{\rm eff}^{SP} &= -\frac{4G_F}{\sqrt{2}}\frac{\alpha_{em}}{4\pi}V_{ts}^*V_{tb}\Big\{R_S\,(\bar{s}P_R b)\,\bar{\mu}\mu + R_P\,(\bar{s}P_R b)\,\bar{\mu}\gamma_5\mu \\
&\qquad + R'_S\,(\bar{s}P_L b)\,\bar{\mu}\mu + R'_P\,(\bar{s}P_L b)\,\bar{\mu}\gamma_5\mu\Big\}\,, \qquad (2.6)\\
\mathcal{H}_{\rm eff}^{T} &= -\frac{4G_F}{\sqrt{2}}\frac{\alpha_{em}}{4\pi}V_{ts}^*V_{tb}\Big\{C_T(\bar{s}\sigma_{\mu\nu}b)\bar{\mu}\sigma^{\mu\nu}\mu + iC_{TE}(\bar{s}\sigma_{\mu\nu}b)\bar{\mu}\sigma_{\alpha\beta}\mu\;\epsilon^{\mu\nu\alpha\beta}\Big\} \qquad (2.7)
\end{aligned}$$

are the new contributions. Here, $R_V, R_A, R'_V, R'_A, R_S, R_P, R'_S, R'_P, C_T$ and C_{TE} are the NP effective couplings. We do not consider NP in the form of the $O_7 = \bar{s}\sigma^{\alpha\beta}P_R b\,F_{\alpha\beta}$ operator or its chirally-flipped counterpart $O'_7 = \bar{s}\sigma^{\alpha\beta}P_L b\,F_{\alpha\beta}$. This is because there has been no hint of NP in the radiative decays $\bar{B} \to X_s\gamma, \bar{K}^{(*)}\gamma$ [45], which imposes strong constraints on $|C_7^{\rm eff}|$. This by itself does not rule out the possibility of a flipped-sign $C_7^{\rm eff}$ scenario. However this solution can be ruled out at 3σ from the decay rate of $\bar{B} \to X_s\ell^+\ell^-$ if there are no NP effects in C_9 and C_{10} [75]. Thus, NP effects exclusively in C_7 cannot provide large deviations from the SM. The impact of O'_7 on the forward-backward asymmetry in $\bar{B}^0_d \to \bar{K}^*\mu^+\mu^-$, together with other observables, was studied in ref. [60].

Note that the operators with coefficients R_V and R_A have the same Lorentz structure as those in the SM involving C_9 and C_{10}, respectively [see eq. (2.1)], so that any measurement will be sensitive only to the combinations $(C_9 + R_V)$ or $(C_{10} + R_A)$. For simplicity, in our numerical analysis of the observables of various decays, these couplings are taken to be real. As a consequence, the results in this paper would be the same if the corresponding CP-conjugate decays were considered. However, for completeness, the expressions allow for a complex-coupling analysis.

When calculating the transition amplitudes, for the leptonic part we use the notation

$$\begin{aligned}
L^\mu &\equiv \langle\mu^+(p_+)\mu^-(p_-)|\bar{\mu}\gamma^\mu\mu|0\rangle, & L^{\mu 5} &\equiv \langle\mu^+(p_+)\mu^-(p_-)|\bar{\mu}\gamma^\mu\gamma^5\mu|0\rangle,\\
L &\equiv \langle\mu^+(p_+)\mu^-(p_-)|\bar{\mu}\mu|0\rangle, & L^5 &\equiv \langle\mu^+(p_+)\mu^-(p_-)|\bar{\mu}\gamma^5\mu|0\rangle, \qquad (2.8)\\
L^{\mu\nu} &\equiv \langle\mu^+(p_+)\mu^-(p_-)|\bar{\mu}\sigma^{\mu\nu}\mu|0\rangle.
\end{aligned}$$

JHEP11(2011)121

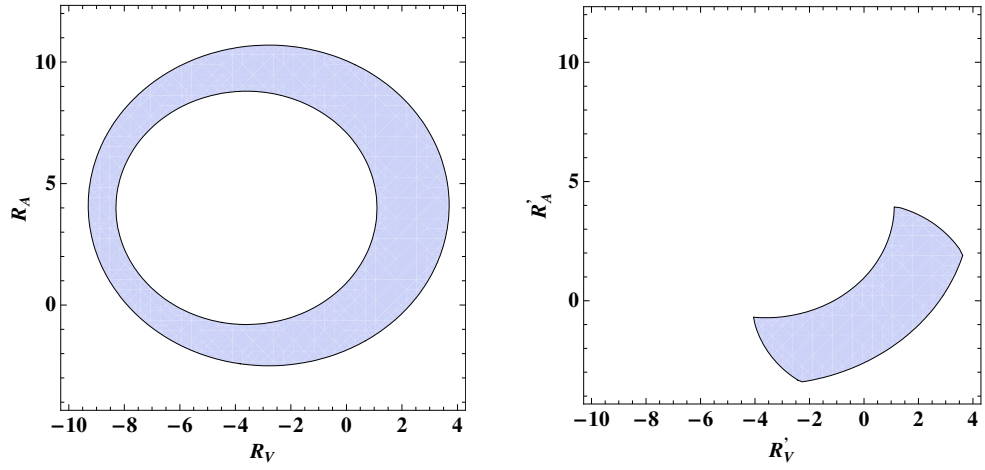

Figure 1. The constraints on the couplings R_V, R_A (left panel) and R'_V, R'_A (right panel) when only primed or unprimed couplings are present.

2.2 Constraints on NP couplings

The constraints on the NP couplings in $b \to s\mu^+\mu^-$ come mainly from the upper bound on the branching ratio $B(\bar{B}_s^0 \to \mu^+\mu^-)$ and the measurements of the total branching ratios $B(\bar{B}_d^0 \to X_s\mu^+\mu^-)$ and $B(\bar{B}_d^0 \to \bar{K}\mu^+\mu^-)$ [76–80]:

$$B(\bar{B}_s^0 \to \mu^+\mu^-) < 3.60 \times 10^{-8} \quad (90\%\ \text{C.L.})\,, \tag{2.9}$$

$$B(\bar{B}_d^0 \to X_s\mu^+\mu^-) = \begin{cases} (1.60 \pm 0.50) \times 10^{-6} & (\text{low } q^2) \\ (0.44 \pm 0.12) \times 10^{-6} & (\text{high } q^2) \end{cases}\,, \tag{2.10}$$

$$B(\bar{B}_d^0 \to \bar{K}\mu^+\mu^-) = \left(4.5^{+1.2}_{-1.0}\right) \times 10^{-7}\,, \tag{2.11}$$

where the low-q^2 and high-q^2 regions correspond to $1\,\text{GeV}^2 \le q^2 \le 6\,\text{GeV}^2$ and $q^2 \ge 14.4\,\text{GeV}^2$, respectively, where q^2 is the invariant mass squared of the two muons. The constraints from the first two quantities above have been derived in ref. [62]. Here we also include the additional constraints from $B(\bar{B}_d^0 \to \bar{K}\mu^+\mu^-)$. The three decays above provide complementary information about the NP operators. For the SM predictions here, we use the latest NNLO calculations. Note that the measurements for $B(\bar{B}_d^0 \to \bar{K}^*\mu^+\mu^-)$ are also available [11, 12]. However, the form-factor uncertainties in $\bar{B}_d^0 \to \bar{K}^*\mu^+\mu^-$ are rather large, and as a result the constraints due to this decay mode are subsumed in those from the other three modes.

The constraints on the new VA couplings come mainly from $B(\bar{B}_d^0 \to X_s\mu^+\mu^-)$ and $B(\bar{B}_d^0 \to \bar{K}\mu^+\mu^-)$. Their precise values depend on which NP operators are assumed to be present. For example, if only $R_{V,A}$ or only $R'_{V,A}$ couplings are present, the constraints on these couplings take the form shown in figure 1. For $R_{V,A}$, the allowed parameter space is the region between two ellipses:

$$1.0 \lesssim \frac{|R_V + 3.6|^2}{(4.7)^2} + \frac{|R_A - 4.0|^2}{(4.8)^2}\,, \quad \frac{|R_V + 2.8|^2}{(6.5)^2} + \frac{|R_A - 4.1|^2}{(6.6)^2} \lesssim 1\,, \tag{2.12}$$

JHEP11(2011)121

while for $R'_{V,A}$, the allowed region is the intersection of an annulus and a circle:

$$22.2 \lesssim |R'_V + 3.6|^2 + |R'_A - 4.0|^2 \lesssim 56.6\,, \quad |R'_V|^2 + |R'_A|^2 \lesssim 17\,. \tag{2.13}$$

If both $R_{V,A}$ and $R'_{V,A}$ are present, the constraints on them get individually weakened to

$$\frac{|R_V + 2.8|^2}{(6.5)^2} + \frac{|R_A - 4.1|^2}{(6.6)^2} \lesssim 1\,, \tag{2.14}$$

and

$$|R'_V|^2 + |R'_A|^2 \lesssim 40\,, \tag{2.15}$$

respectively.[2]

For the SP operators, the present upper bound on $B(\bar{B}^0_s \to \mu^+\mu^-)$ provides the limit

$$|R_S - R'_S|^2 + |R_P - R'_P|^2 \lesssim 0.44\,, \tag{2.16}$$

where we have used $f_{B_s} = (238.8 \pm 9.5)\,\text{MeV}$ [81] and $|V^*_{ts}V_{tb}| = 0.0407 \pm 0.0010$ [77]. This constitutes a severe constraint on the NP couplings if only $R_{S,P}$ or $R'_{S,P}$ are present. However, if both types of operators are present, these bounds can be evaded due to cancellations between the $R_{S,P}$ and $R'_{S,P}$. In that case, $B(\bar{B}^0_d \to X_s\mu^+\mu^-)$ and $B(\bar{B}^0_d \to \bar{K}\mu^+\mu^-)$ can still bound these couplings. The stronger bound is obtained from the measurement of the latter quantity, which yields

$$|R_S|^2 + |R_P|^2 \lesssim 9\,, \quad R_S \approx R'_S\,, \quad R_P \approx R'_P\,. \tag{2.17}$$

Finally, the constraints on the NP tensor operators come entirely from $B(\bar{B}^0_d \to X_s\mu^+\mu^-)$. When only the T operators are present,

$$|C_T|^2 + 4|C_{TE}|^2 \lesssim 1.0\,. \tag{2.18}$$

Although the bounds presented in this section for VA, SP and T couplings are obtained by taking one kind of Lorentz structure at a time, in our numerical analysis for scenarious where we consider combinations of two or more kinds of Lorentz structres, we use the allowed parameter space obtained by considering the corresponding combined Lorentz structures.

We now analyze the $b \to s\mu^+\mu^-$ modes in detail and present our results. As explained in the Introduction, the figures have the SM prediction bands overlaid with the predictions for specific allowed values of NP couplings. The SM band is generated by varying the form factors within their ranges as predicted by the respective authors, while the CKM matrix elements, quark masses and meson decay constants are varied within their 1.6σ allowed values.

[2]Note: the constraints on $R_{V,A}$ obtained here are milder than those obtained in ref. [43] using $B(\bar{B}^0_d \to (\bar{K}\,, \bar{K}^*)\,\mu^+\,\mu^-)$. This is because ref. [43] had neglected the interference terms between the SM and new physics VA operators. Their inclusion relaxes the stringent constraints therein.

JHEP11(2011)121

3 $\bar{B}_s^0 \to \mu^+\mu^-$

In this section we examine the NP contributions to $\bar{B}_s^0 \to \mu^+\mu^-$. Within the SM, $\bar{B}_s^0 \to \mu^+\mu^-$ is chirally suppressed. The SM prediction for the branching ratio is $B(\bar{B}_s^0 \to \mu^+\mu^-) = (3.35 \pm 0.32) \times 10^{-9}$ [22]. The Tevatron gives an upper bound on its branching ratio (BR) of 3.6×10^{-8} at 90% C.L. [76–78]. This decay can be observed at the Tevatron only if NP enhances its BR above 10^{-8}. LHCb is the only experiment which will probe $B(\bar{B}_s^0 \to \mu^+\mu^-)$ down to its SM value. It has the potential for a 3σ observation (5σ discovery) of $\bar{B}_s^0 \to \mu^+\mu^-$ with ~ 2 fb^{-1} (~ 6 fb^{-1}) of data [82]. LHCb therefore has the potential to observe either an enhancement or a suppression of $B(\bar{B}_s^0 \to \mu^+\mu^-)$. It can observe $\bar{B}_s^0 \to \mu^+\mu^-$ as long as its BR is above 1.0×10^{-9}.

3.1 Branching ratio

The transition amplitude for $\bar{B}_s^0 \to \mu^+\mu^-$ is given by

$$\begin{aligned} i\mathcal{M}(\bar{B}_s^0 \to \mu^+\mu^-) = (-i)\frac{1}{2}\Big[-\frac{4G_F}{\sqrt{2}}\frac{\alpha_{em}}{4\pi}(V_{ts}^* V_{tb})\Big] \times \\ \Big\{ \langle 0\,|\bar{s}\gamma_\mu\gamma_5 b|\,\bar{B}_s^0(p)\rangle\,(-C_{10}^{\rm eff} - R_A + R'_A)L^{5\mu} \\ + \langle 0\,|\bar{s}\gamma_5 b|\,\bar{B}_s^0(p)\rangle\,\left[(R_S - R'_S)L + (R_P - R'_P)L^5\right]\Big\}\,, \end{aligned} \tag{3.1}$$

where $L^{5\mu}$, L and L^5 are defined in eq. (2.8). Using the matrix elements [15]

$$\langle 0\,|\bar{s}\gamma_\mu\gamma_5 b|\,\bar{B}_s^0(p)\rangle = i\,p_\mu\,f_{B_s}\,, \quad \langle 0\,|\bar{s}\gamma_5 b|\,\bar{B}_s^0(p)\rangle = -i\,f_{B_s}\frac{m_{B_s}^2}{m_b + m_s}\,, \tag{3.2}$$

the calculation of the BR gives

$$\begin{aligned} B(\bar{B}_s^0 \to \mu^+\,\mu^-) = \frac{G_F^2\alpha_{em}^2 m_{B_s}^5 f_{B_s}^2 \tau_{B_s}}{64\pi^3}|V_{tb}V_{ts}^*|^2\sqrt{1-\frac{4m_\mu^2}{m_{B_s}^2}} \times \\ \left\{\left(1-\frac{4m_\mu^2}{m_{B_s}^2}\right)\left|\frac{R_S - R'_S}{m_b+m_s}\right|^2 + \left|\frac{R_P - R'_P}{m_b+m_s} + \frac{2m_\mu}{m_{B_s}^2}(C_{10} + R_A - R'_A)\right|^2\right\}. \end{aligned} \tag{3.3}$$

Clearly, NP in the form of tensor operators does not contribute to $\bar{B}_s^0 \to \mu^+\mu^-$. From eq. (3.3) and the constraints on NP couplings obtained in section 2.2, one can study the effect of new VA and SP couplings.

Since the NP contribution from VA operators is suppressed by a factor of $\sim m_\mu/m_b$ compared to that from the SP operators, the effect of SP operators dominates. Both VA and SP operators can suppress $B(\bar{B}_s^0 \to \mu^+\mu^-)$ significantly below the SM prediction. However while VA operators can only marginally enhance $B(\bar{B}_s^0 \to \mu^+\mu^-)$ above 10^{-8}, making the decay accessible at the Tevatron in an optimistic scenario, the SP operators can enhance the branching ratio even up to the present experimental bound. Indeed, the strongest limit on the SP couplings comes from this decay. This strong limit prevents the SP operators from expressing themselves in many other observables, as we shall see later in this paper.

JHEP11(2011)121

3.2 Muon polarization asymmetry

The longitudinal polarization asymmetry of muons in $\bar{B}_s^0 \to \mu^+\mu^-$ is defined as

$$A_{LP} = \frac{N_R - N_L}{N_R + N_L}\,, \tag{3.4}$$

where $N_R\,(N_L)$ is the number of μ^-'s emerging with positive (negative) helicity. A_{LP} is a clean observable that is not suppressed by m_μ/m_{B_s} only if the NP contribution is in the form of SP operators, such as in an extended Higgs sector.

A_{LP} for the most general NP is [70]

$$A_{LP} = \frac{2\sqrt{1-\frac{4m_\mu^2}{m_{B_s}^2}}\,\mathrm{Re}\left[\left(\frac{R_S-R'_S}{m_b+m_s}\right)\left(\frac{R_P-R'_P}{m_b+m_s}+\frac{2m_\mu}{m_{B_s}^2}(C_{10}+R_A-R'_A)\right)\right]}{\left(1-\frac{4m_\mu^2}{m_{B_s}^2}\right)\left|\frac{R_S-R'_S}{m_b+m_s}\right|^2+\left|\frac{R_P-R'_P}{m_b+m_s}+\frac{2m_\mu}{m_{B_s}^2}(C_{10}+R_A-R'_A)\right|^2}\,. \tag{3.5}$$

From the above equation, we see that A_{LP} can be nonzero if and only if $R_S - R'_S \neq 0$, i.e. there must be a contribution from NP SP operators. (Within the SM, SP couplings are negligibly small, so that $A_{LP} \simeq 0$.)

The present upper bound on $B(\bar{B}_s^0 \to \mu^+\mu^-)$ puts no constraint on A_{LP}, and it can be as large as 100% [70]. A_{LP} can be maximal even if $B(\bar{B}_s^0 \to \mu^+\mu^-)$ is close to its SM prediction. Therefore, in principle A_{LP} can serve as an important tool to probe NP of the SP form. However, in order to measure its polarization, the muon must decay within the detector. This is not possible due to the long muon lifetime ($c\tau$ for the muon is 659 m). Hence in practice, this quantity is not measurable at current detectors.

4 $\bar{B}_d^0 \to X_s\mu^+\mu^-$

The BR of $\bar{B}_d^0 \to X_s\mu^+\mu^-$ in the low-q^2 and high-q^2 regions has been measured to be [79, 80]

$$B(\bar{\mathrm{B}} \to X_s\ell^+\ell^-)_{\text{low } q^2} = \begin{cases} \left(1.49 \pm 0.50^{+0.41}_{-0.32}\right) \times 10^{-6}\,, & \text{(Belle)}\,, \\ (1.8 \pm 0.7 \pm 0.5) \times 10^{-6}\,, & \text{(BaBar)}\,, \\ (1.60 \pm 0.50) \times 10^{-6}\,, & \text{(Average)}\,. \end{cases} \tag{4.1}$$

$$B(\bar{B} \to X_s\ell^+\ell^-)_{\text{high } q^2} = \begin{cases} \left(0.42 \pm 0.12^{+0.06}_{-0.07}\right) \times 10^{-6}\,, & \text{(Belle)}\,, \\ \left(0.50 \pm 0.25^{+0.08}_{-0.07}\right) \times 10^{-6}\,, & \text{(BaBar)}\,, \\ (0.44 \pm 0.12) \times 10^{-6}\,, & \text{(Average)}\,. \end{cases} \tag{4.2}$$

The SM predictions for $B(\bar{B} \to X_s\,\mu^+\,\mu^-)$ in the low-q^2 and high-q^2 regions are $(1.59 \pm 0.11) \times 10^{-6}$ and $(0.24 \pm 0.07) \times 10^{-6}$, respectively [33].

Apart from the measurement of the total BR of $\bar{B}_d^0 \to X_s\mu^+\mu^-$, which has already been used to restrict the VA and T operators in section 2.2, the differential branching ratio (DBR) as a function of q^2 also contains valuable information that can help us detect NP. In particular, the SM predicts a positive zero crossing for A_{FB} in $\bar{B}_d^0 \to X_s\mu^+\mu^-$ in the low-q^2 region, i.e. for q^2 less than (greater than) the crossing point, the value of A_{FB} is negative (positive). This zero crossing is sufficiently away from the charm resonances

JHEP11(2011)121

so that its value can be determined perturbatively to an accuracy of $\sim 5\%$. The NNLO prediction [33] for the zero of $A_{FB}(q^2)$ is (taking $m_b = 4.8\,\text{GeV}$)

$$(q^2)_0 = (3.5 \pm 0.12)\,\text{GeV}^2\,. \tag{4.3}$$

This quantity has not yet been measured. However, estimates show that a precision of about 5% could be obtained at a Super-B factory [83]. A deviation from the zero crossing point predicted above will be a clear signal of NP.

4.1 Differential branching ratio and forward-backward asymmetry

After including all the NP interactions, and neglecting terms suppressed by m_μ/m_b and m_s/m_b, the total differential branching ratio $\mathrm{d}B/\mathrm{d}z$ is given by

$$\left(\frac{\mathrm{d}B}{\mathrm{d}z}\right)_{\text{Total}} = \left(\frac{\mathrm{d}B}{\mathrm{d}z}\right)_{\text{SM}} + B_0\Big[B_{\text{SM-}VA} + B_{VA} + B_{SP} + B_T\Big]\,, \tag{4.4}$$

where the quantities B depend on the SM and NP couplings and kinematic variables. The complete expressions for these quantities are given in appendix A. The subscripts denote the Lorentz structure(s) contributing to that term.

The forward-backward asymmetry in $\bar{B}^0_d \to X_s\mu^+\mu^-$ is

$$A_{FB}(q^2) = \frac{\int_0^1 d\cos\theta_\mu \frac{d^2B}{dq^2 d\cos\theta_\mu} - \int_{-1}^0 d\cos\theta_\mu \frac{d^2B}{dq^2 d\cos\theta_\mu}}{\int_0^1 d\cos\theta_\mu \frac{d^2B}{dq^2 d\cos\theta_\mu} + \int_{-1}^0 d\cos\theta_\mu \frac{d^2B}{dq^2 d\cos\theta_\mu}}\,, \tag{4.5}$$

where θ_μ is the angle between the μ^+ and the $\bar{B}^0$ in the dimuon center-of-mass frame. We can write A_{FB} in the form

$$A_{FB}(q^2) = \frac{N(z)}{\mathrm{d}B/\mathrm{d}z}\,, \tag{4.6}$$

where the numerator is given by

$$N(z) = B_0\Big[N_{\text{SM}} + N_{\text{SM-}VA} + N_{VA} + N_{SP\text{-}T}\Big]\,. \tag{4.7}$$

The terms suppressed by m_μ/m_b and m_s/m_b have been neglected as before. Again for the detailed expressions, we refer the reader to appendix A.

Figure 2 shows $A_{FB}(q^2)$ and the DBR for $\bar{B}^0_d \to X_s\mu^+\mu^-$ in the presence of NP in the form of $R_{V,A}$ couplings, which are the ones that can most influence these observables. Enhancement or suppression of the DBR by a factor of 2 is possible. The NP couplings can enhance A_{FB} up to 30% at low q^2, make it have either sign, and even make the zero crossing disappear altogether. At high q^2, however, A_{FB} can only be suppressed. The $R'_{V,A}$ couplings can only affect these observables mildly: a 50% enhancement in DBR is possible (no suppression), but A_{FB} can only be marginally enhanced and a positive zero crossing in the $q^2 = 2\text{-}4\,\text{GeV}^2$ region is maintained. The mild effect of $R'_{V,A}$ couplings as compared to the $R_{V,A}$ couplings is a generic feature for almost all observables. This may be attributed to the bounds on the magnitudes of these couplings: from section 2.2, while $|R_{V,A}| < 10$, the values of $|R'_{V,A}| < 5$.

JHEP11(2011)121

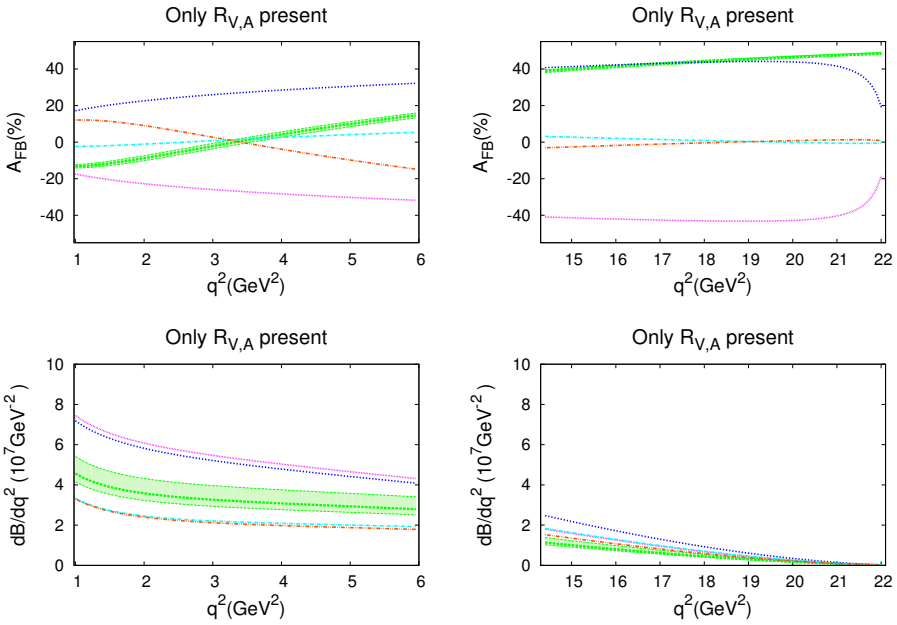

Figure 2. The left (right) panels of the figure show A_{FB} and DBR for $\bar{B}^0_d \to X_s\mu^+\mu^-$ in the low-q^2 (high-q^2) region, in the scenario where only (R_V, R_A) terms are present. The band corresponds to the SM prediction and its uncertainties; the lines show predictions for some representative values of NP parameters (R_V, R_A). For example, the blue curves in the low-q^2 and high-q^2 regions correspond to $(-6.85, 8.64)$ and $(-9.34, 8.85)$, respectively.

Eq. (4.7) shows that if SP or T couplings are individually present, their contribution to A_{FB} is either absent or suppressed by m_μ/m_b. In such a case, though they can enhance the DBR (marginally for SP, by up to a factor of 2 for T), A_{FB} is suppressed in general (marginally for SP, significantly for T). However if both SP and T operators are present, their interference term is not suppressed and some enhancement of A_{FB} is possible. This still is not significant, since the magnitude of the SP couplings is highly constrained from $\bar{B}^0_s \to \mu^+\mu^-$ measurements. A positive zero crossing in the low-q^2 region is always maintained. This may be seen in figure 3.

4.2 Polarization fractions f_L and f_T

In ref. [34] it was pointed out that, besides the dilepton invariant mass spectrum and the forward-backward asymmetry, a third observable can be obtained from $\bar{B}^0_d \to X_s\mu^+\mu^-$, namely the double differential decay width:

$$\frac{d^2B}{dz\, d\cos\theta_\mu} = \frac{3}{8}\Big[(1+\cos^2\theta_\mu)H_T(z) + 2\cos\theta_\mu H_A(z) + 2(1-\cos^2\theta_\mu)H_L(z)\Big]\,. \qquad (4.8)$$

The functions $H_i(z)$ do not depend on $\cos\theta_\mu$. The sum $H_L(z) + H_T(z)$ gives the differential branching ratio dB/dz, while the forward-backward asymmetry is given by $3\,H_A/4(H_L + H_T)$. Splitting dB/dz into longitudinal and transverse parts separates the contributions with different q^2 dependences, providing a third independent observable.

JHEP11(2011)121

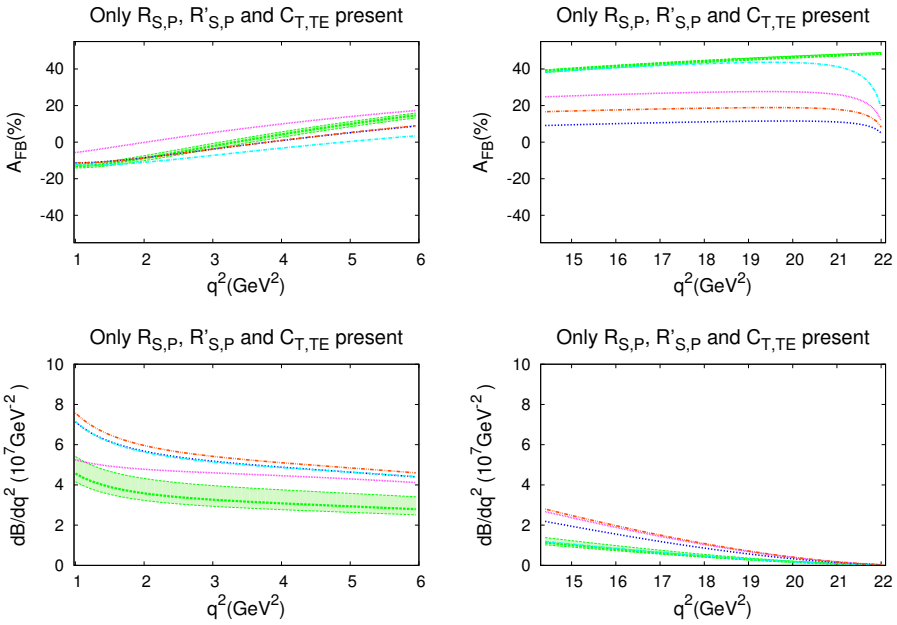

Figure 3. The left (right) panels of the figure show A_{FB} and DBR for $\bar{B}_d^0 \to X_s\mu^+\mu^-$ in the low-q^2 (high-q^2) region, in the scenario where both SP and T terms are present. The band corresponds to the SM prediction and its uncertainties; the lines show predictions for some representative values of NP parameters $(R_S, R_P, R'_S, R'_P, C_T, C_{TE})$. For example, the magenta curves in the low-q^2 and high-q^2 regions correspond to $(-1.23, -1.79, -0.86, -1.85, 0.27, -0.36)$ and $(-1.23, -0.23, -1.35, 0.08, 1.37, 0.01)$, respectively.

This does not require measuring any additional kinematical variable — q^2 and $\cos\theta_\mu$ are sufficient. Including all the NP interactions, and neglecting terms suppressed by m_μ/m_b and m_s/m_b, $H_L(z)$ and $H_T(z)$ are given by

$$H_L(z) = H_L^{\rm SM}(z) + H_L^{{\rm SM}-VA}(z) + H_L^{VA}(z) + H_L^{SP}(z) + H_L^{T}(z)\,, \tag{4.9}$$

$$H_T(z) = H_T^{\rm SM}(z) + H_T^{{\rm SM}-VA}(z) + H_T^{VA}(z) + H_T^{SP}(z) + H_T^{T}(z)\,, \tag{4.10}$$

where the H functions are given in appendix A. The superscripts indicate the Lorentz structures contributing to the term. The polarization fractions f_L and f_T can be defined as

$$f_L = \frac{H_L(z)}{H_L(z)+H_T(z)}\,, \qquad f_T = \frac{H_T(z)}{H_L(z)+H_T(z)}\,. \tag{4.11}$$

In the SM, f_L can be as large as 0.9 at low q^2, and it decreases to about 0.3 at high q^2.

Figure 4 shows that when only $R_{V,A}$ couplings are present, in the low-q^2 region f_L can be suppressed substantially, or even enhanced up to 1. A similar effect — small enhancement or a factor of two suppression — is possible at high q^2. The suppression at low-q^2 is typically correlated with an enhancement at high-q^2. The effect of $R'_{V,A}$ couplings is similar, but much milder, as expected. SP and T operators, individually or together, can only have an marginal effect on f_L.

JHEP11(2011)121

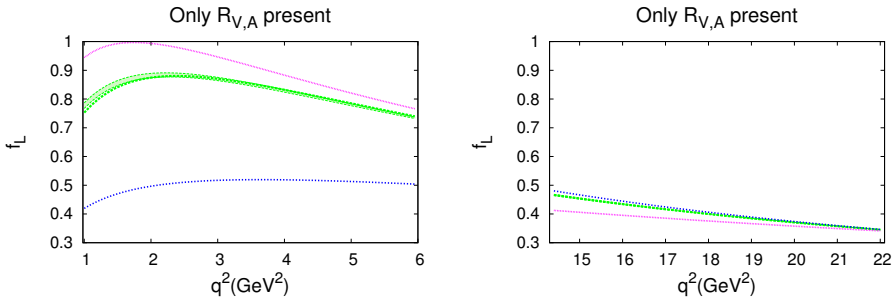

Figure 4. The left (right) panels of the figure show f_L for $\bar{B}_d^0 \to X_s\mu^+\mu^-$ in the low-q^2 (high-q^2) region, in the scenario where only (R_V, R_A) terms are present. The band corresponds to the SM prediction and its uncertainties; the lines show predictions for some representative values of NP parameters (R_V, R_A). For example, the blue curves in the low-q^2 and high-q^2 regions correspond to $(-8.14, 5.75)$ and $(1.87, 4.85)$, respectively.

5 $\bar{B}_s^0 \to \mu^+\mu^-\gamma$

In this section we examine the NP contributions to the radiative leptonic decay $\bar{B}_s^0 \to \mu^+\mu^-\gamma$. This decay has not been detected as yet. The SM prediction for the BR in the range $q^2 \leq 9.5\,\text{GeV}^2$ and $q^2 \geq 15.9\,\text{GeV}^2$ is $\approx 18.9 \times 10^{-9}$ [41]. Although this decay needs the emission of an additional photon as compared to $\bar{B}_s^0 \to \mu^+\mu^-$, which would suppress the BR by a factor of α_{em}, the photon emission also frees it from helicity suppression, making its BR much larger than $\bar{B}_s^0 \to \mu^+\mu^-$.

This decay has contributions from many channels [36–39, 41, 42]: (i) direct emission of real or virtual photons from valence quarks of the $\bar{B}_s^0$, (ii) real photon emitted from an internal line of the $b \to s$ loop, (iii) weak annihilation due to the axial anomaly, and (iv) bremsstrahlung from leptons in the final state. The photon emission from the $b \to s$ loop is suppressed by m_b^2/m_W^2 [37], and the weak annihilation is further suppressed by Λ_{QCD}/m_b [41]. These two contributions can then be neglected. The bremsstrahlung contribution is suppressed by m_μ/m_b, and dominates only at extremely low photon energies due to the infrared divergence. The virtual photon emission dominates in the low-q^2 region around the ϕ resonance. If we choose the regions $2\,\text{GeV}^2 \leq q^2 \leq 6\,\text{GeV}^2$ and $14.4\,\text{GeV}^2 \leq q^2 \leq 25\,\text{GeV}^2$ as the low-q^2 and high-q^2 regions, respectively, then the dominating contribution comes from the diagrams in which the final-state photon is emitted either from the b or the s quark. Then the $\bar{B}_s^0 \to \mu^+\mu^-\gamma$ decay is governed by the effective Hamiltonian describing the $b \to s\mu^+\mu^-$ transition, as given in eq. (2.1), and our formalism is applicable. Here we consider the the DBR and A_{FB} in $\bar{B}_s^0 \to \mu^+\mu^-\gamma$.

5.1 Differential branching ratio and forward-backward asymmetry

We begin with the differential branching ratio. The SP operators do not contribute to the amplitude of $\bar{B}_s^0 \to \mu^+\mu^-\gamma$ and hence do not play any role in the decay.

In terms of the dimensionless parameter $x_\gamma = 2E_\gamma/m_{B_s}$, where E_γ is the photon energy

JHEP11(2011)121

in the $\bar{B}_s^0$ rest frame, one can calculate the double differential decay rate to be

$$\frac{\mathrm{d}^2\Gamma}{\mathrm{d}x_\gamma \mathrm{d}(\cos\theta_\mu)} = \frac{1}{2m_{B_s}} \frac{2v\, m_{B_s}^2 x_\gamma}{(8\pi)^3} \mathcal{M}^\dagger \mathcal{M} \,, \tag{5.1}$$

where $v \equiv \sqrt{1 - 4m_\mu^2/[m_{B_s}^2(1-x_\gamma)]}$. From eq. (5.1) we get the DBR to be

$$\begin{aligned} \frac{\mathrm{d}B}{\mathrm{d}x_\gamma} &= \tau_{B_s} \int_{-1}^{1} \frac{\mathrm{d}^2\Gamma}{\mathrm{d}x_\gamma \mathrm{d}(\cos\theta_\mu)} \mathrm{d}\cos\theta_\mu \\ &= \tau_{B_s} \left[\frac{1}{2m_{B_s}} \frac{2vm_{B_s}^2}{(8\pi)^3}\right] \left[\frac{1}{4}\, \frac{16G_F^2}{2} \frac{\alpha_{em}^2}{16\pi^2} |V_{tb}V_{ts}^*|^2 e^2\right] \Theta \,. \end{aligned} \tag{5.2}$$

Here the quantity Θ has the form

$$\Theta = \frac{2}{3}\, m_{B_s}^4\, x_\gamma^3 \Big[X_{VA} + X_T + X_{VA\text{-}T}\Big] \,, \tag{5.3}$$

where the X terms are given in appendix B. The subscripts of the X terms denote the Lorentz structure(s) contributing to that term. For the sake of brevity, we have included the SM contributions in X_{VA}.

The normalized forward-backward asymmetry of muons in $\bar{B}_s^0 \to \mu^+\mu^-\gamma$ is defined as

$$A_{FB}(q^2) = \frac{\displaystyle\int_0^1 d\cos\theta_\mu \frac{d^2B}{dq^2 d\cos\theta_\mu} - \int_{-1}^0 d\cos\theta_\mu \frac{d^2B}{dq^2 d\cos\theta_\mu}}{\displaystyle\int_0^1 d\cos\theta_\mu \frac{d^2B}{dq^2 d\cos\theta_\mu} + \int_{-1}^0 d\cos\theta_\mu \frac{d^2B}{dq^2 d\cos\theta_\mu}} \,, \tag{5.4}$$

where θ_μ is the angle between the three-momentum vectors of the $\bar{B}_s^0$ and the μ^+ in the dimuon center-of-mass frame. The calculation of A_{FB} gives

$$A_{FB}(q^2) = \frac{1}{\Theta} \left(2m_{B_s}^4 v\, x_\gamma^3\right) \Big[Y_{VA} + Y_{VA\text{-}T}\Big] \,, \tag{5.5}$$

with the Y terms are defined in appendix B.

The details of the calculation are given in appendix B. For the numerical calculations, we use the matrix elements given in ref. [40]. The parameters involved in the form factor calculations are chosen in such a way that the LEET relations between form factors are satisfied to a 10% accuracy [40]. In our numerical analysis we take the errors in these form factors to be $\pm 10\%$.

Within the SM, $A_{FB}(q^2)$ is predicted to vanish around $q^2 \approx 4.3\,\mathrm{GeV}^2$ (i.e. $x_\gamma \approx 0.85$) [40], and the crossing is predicted to be negative. It is therefore interesting to see the effects of various NP operators and their combinations on A_{FB}. In the extreme LEET limit, using the form-factor relations given in ref. [40], one can easily see that the A_{FB} is independent of the form factors. In figure 5 we see large bands in the SM predictions of A_{FB} in the low q^2 region. One may tend to interpret these as large corrections to the LEET limit, however this would be somewhat misleading, as we take the errors in the form factors, due to corrections from the LEET limit, to be uncorrelated. In realistic models,

JHEP11(2011)121

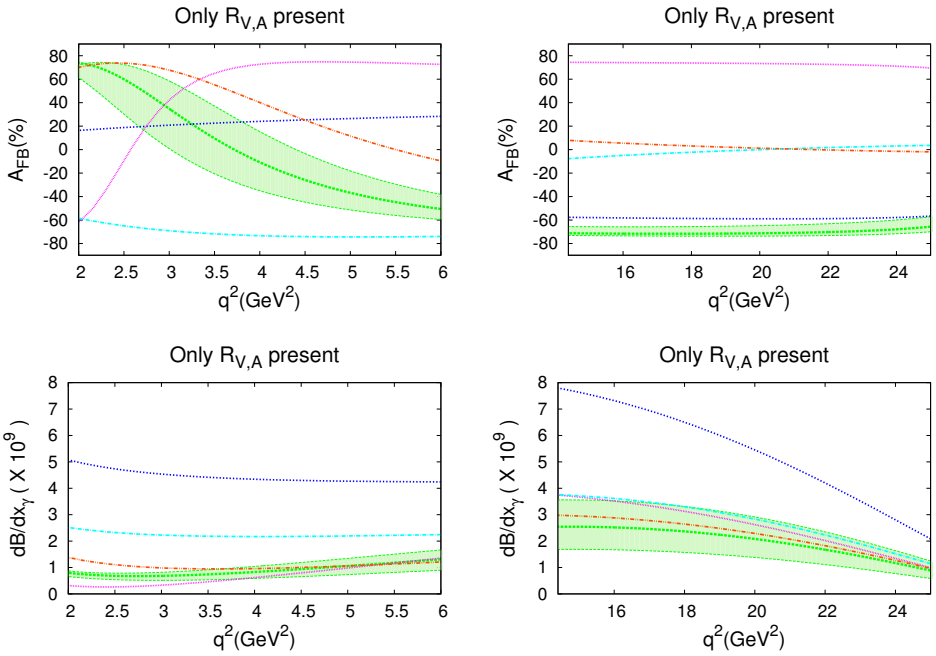

Figure 5. The left (right) panels of the figure show A_{FB} and DBR for $\bar{B}_s^0 \to \mu^+\mu^-\gamma$ in the low-q^2 (high-q^2) region, in the scenario where only (R_V, R_A) terms are present. Note that here $q^2 = m_B^2(1 - x_\gamma)$. The band corresponds to the SM prediction and its uncertainties; the lines show predictions for some representative values of NP parameters (R_V, R_A). For example, the magenta curves in the low-q^2 and high-q^2 regions correspond to $(2.47, 7.08)$ and $(-7.14, -0.42)$, respectively.

LEET corrections to the form factors will be correlated, leading to a smaller uncertainty band for A_{FB} in the SM.

Figure 5 also shows A_{FB} and DBR in the presence of NP in the form of $R_{V,A}$ couplings. With the large allowed values of $|R_{V,A}|$ and the absence of any helicity suppression, we expect VA operators to have a significant impact on the observables. As can be seen from the figure, the maximum allowed value of DBR can be 2-3 times larger than the SM prediction. The BR can also be suppressed below the SM prediction due to destructive interference. In the low-q^2 region, the suppression can be large. The features of the zero-crossing predicted by the SM can be affected: it can be positive or negative, can take place at any value of q^2, and can disappear altogether. As expected, the impact of $R'_{V,A}$ couplings is much milder. In particular, the zero-crossing is always positive and in the low-q^2 region.

With new tensor couplings, an enhancement of the DBR by up to a factor of 3 in comparison to the SM prediction is possible. Moreover, in the limit of neglecting the muon mass, T operators do not contribute to the Y-terms in eq. (5.5); their contribution is only to Θ. As a result, they can only suppress A_{FB} from its SM value.

When all NP operators are allowed, we find that $B(\bar{B}_s^0 \to \mu^+\mu^-\gamma)$ can be enhanced by a factor of 4, or it can be suppressed significantly. The shape of $A_{FB}(q^2)$ is determined by the new VA couplings, while its magnitude can be suppressed if the T couplings are significant.

JHEP11(2011)121

6 $\bar{B}^0_d \to \bar{K}\mu^+\mu^-$

The decay mode $\bar{B}^0_d \to \bar{K}\mu^+\mu^-$ is interesting primarily because the forward-backward asymmetry of muons is predicted to vanish in the SM. This is due to the fact that the hadronic matrix element for the $\bar{B}^0_d \to \bar{K}$ transition does not have any axial-vector contribution. A_{FB} can have a nonzero value only if it receives a contribution from new physics in the form of SP or T operators. Thus, the information from this decay is complementary to that from the other decays considered earlier, which were more sensitive to new physics VA operators.

The total branching ratio of $\bar{B}^0_d \to \bar{K}\mu^+\mu^-$ has been measured to be [78]

$$B(\bar{B}^0_d \to \bar{K}\mu^+\mu^-) = \left(4.5^{+1.2}_{-1.0}\right) \times 10^{-7}\,, \tag{6.1}$$

which is consistent with the SM prediction [32]

$$B(\bar{B}^0_d \to \bar{K}\mu^+\mu^-)_{\rm SM} = (3.5 \pm 1.2) \times 10^{-7}\,. \tag{6.2}$$

The integrated asymmetry, $\langle A_{FB}\rangle$, has been measured by BaBar [84] and Belle [10, 85] to be

$$\langle A_{FB}\rangle = (0.15^{+0.21}_{-0.23} \pm 0.08) \qquad \text{(BaBar)}\,, \tag{6.3}$$

$$\langle A_{FB}\rangle = (0.10 \pm 0.14 \pm 0.01) \qquad \text{(Belle)}. \tag{6.4}$$

These measurements are consistent with zero. However, within 2σ they can be as large as $\sim 40\%$. Experiments such as the LHC or a future Super-B factory will increase the statistics by more than two orders of magnitude. For example, at ATLAS at the LHC, after analysis cuts the number of $\bar{B}^0_d \to \bar{K}\mu^+\mu^-$ events is expected to be ~ 4000 with $30\,\text{fb}^{-1}$ of data [86]. Thus, $\langle A_{FB}\rangle$ can soon be probed to values as low as 5%. With higher statistics, one will even be able to measure A_{FB} as a function of the invariant dimuon mass squared q^2. This can provide a stronger handle on this quantity than just its average value $\langle A_{FB}\rangle$.

The effect of NP on $\langle A_{FB}\rangle$ and the $A_{FB}(q^2)$ distribution in $\bar{B}^0_d \to \bar{K}\mu^+\mu^-$ was studied in refs. [48] and [49] respectively. In the latter, it was shown that simultaneous new-physics SP and T operators can lead to a large enhancement of $A_{FB}(q^2)$ in the high-q^2 region. However, NP effects due to other operators were not studied. Here we present a complete analysis of the effect of NP on the $A_{FB}(q^2)$ distribution in $\bar{B}^0_d \to \bar{K}\mu^+\mu^-$ by taking into account all possible NP operators and their combinations. In addition, we study the possible zero crossing of $A_{FB}(q^2)$ and the correlations between the DBR and A_{FB} features.

6.1 Differential branching ratio and forward-backward asymmetry

The differential branching ratio for this mode is given by

$$\frac{dB}{dz} = B'_0\, \phi^{1/2}\, \beta_\mu \Big[X'_{VA} + X'_{SP} + X'_T + X'_{VA\text{-}SP} + X'_{VA\text{-}T}\Big]\,, \tag{6.5}$$

where the normalization factor B'_0, the phase factor ϕ and the X' terms are given in appendix C. The subscripts for the X' terms denote the Lorentz structure(s) contributing to that term.

JHEP11(2011)121

The normalized forward-backward asymmetry for the muons in $\bar{B}_d^0 \to \bar{K}\mu^+\mu^-$ is defined as

$$A_{FB}(q^2) = \frac{\displaystyle\int_0^1 d\cos\theta_\mu \frac{d^2B}{dq^2 d\cos\theta_\mu} - \int_{-1}^0 d\cos\theta_\mu \frac{d^2B}{dq^2 d\cos\theta_\mu}}{\displaystyle\int_0^1 d\cos\theta_\mu \frac{d^2B}{dq^2 d\cos\theta_\mu} + \int_{-1}^0 d\cos\theta_\mu \frac{d^2B}{dq^2 d\cos\theta_\mu}}, \tag{6.6}$$

where θ_μ is the angle between the three-momenta of the $\bar{B}_d^0$ and the μ^+ in the dimuon center-of-mass frame. The calculation of $A_{FB}(q^2)$ gives

$$A_{FB}(q^2) = \frac{2B_0'\,\beta_\mu\,\phi}{dB/dz}\Big[Y'_{VA\text{-}SP} + Y'_{VA\text{-}T} + Y'_{SP\text{-}T}\Big] \tag{6.7}$$

where the Y terms are given in appendix C.

The largest source of uncertainty in the calculations are the $\bar{B} \to \bar{K}$ form factors. As these cannot be calculated from first principles within QCD, one has to rely on models. In the numerical calculations, we use the form factors as calculated in ref. [45] in the framework of QCD light-cone sum rules; the details are given in appendix C. There are, however, certain limits in which relations between form factors can be rigorously obtained. In the large energy (LEET) limit, these relations are valid up to α_s, $1/E_K$ and $1/m_b$ corrections [50, 51].

In the LEET limit, using the form-factor relations in eq. (C.10), one can verify that A_{FB} is independent of the form factors. This is quite useful as it implies that the measurement of A_{FB} can be used to extract the parameters of the new-physics operators without form-factor uncertainties in this limit.

In the low-energy, large q^2, region one can also derive relations between form factors in the heavy-quark limit [73, 74]. However, these relations do not completely eliminate the form-factor dependence of the calculated quantities, and hence we do not consider these relations. An analysis where these relations have been used in the context of $b \to s\mu^+\mu^-$ can be found in refs. [64, 66].

From eq. (6.7), clearly new VA couplings alone cannot give rise to A_{FB}, which vanishes in the SM in any case. Note that this is one of the few cases where the VA couplings fail to influence an asymmetry significantly, in spite of the large allowed values of the couplings. This is because the argument about the hadronic matrix element $\bar{B}_d^0 \to \bar{K}$ not having any axial-vector contribution stays valid even in the presence of NP. The DBR can, however, be enhanced by up to a factor of 2, or marginally suppressed.

The contribution of SP operators through the $Y'_{VA\text{-}SP}$ terms can give rise to A_{FB}, where the VA contribution comes from the SM operators. The effect is rather small when only $R_{S,P}$ or only $R'_{S,P}$ couplings are present, due to the strong constraints on their values. The peak value of A_{FB} in the low-q^2 region stays below the percent level, while in the the high-q^2 region it can be enhanced up to 2% at the extreme end point ($q^2 \gtrsim 22\,\text{GeV}^2$), which is virtually impossible to observe. However if both the primed and unprimed SP couplings are present simultaneously, the constraints on them are weakened. In such a situation, the peak value of A_{FB} in the low-q^2 (high-q^2) can become $\sim 5\%$ ($\sim 3\%$). This may be seen in figure 6. It is also observed that A_{FB} is always positive or always negative, i.e. there is no

JHEP11(2011)121

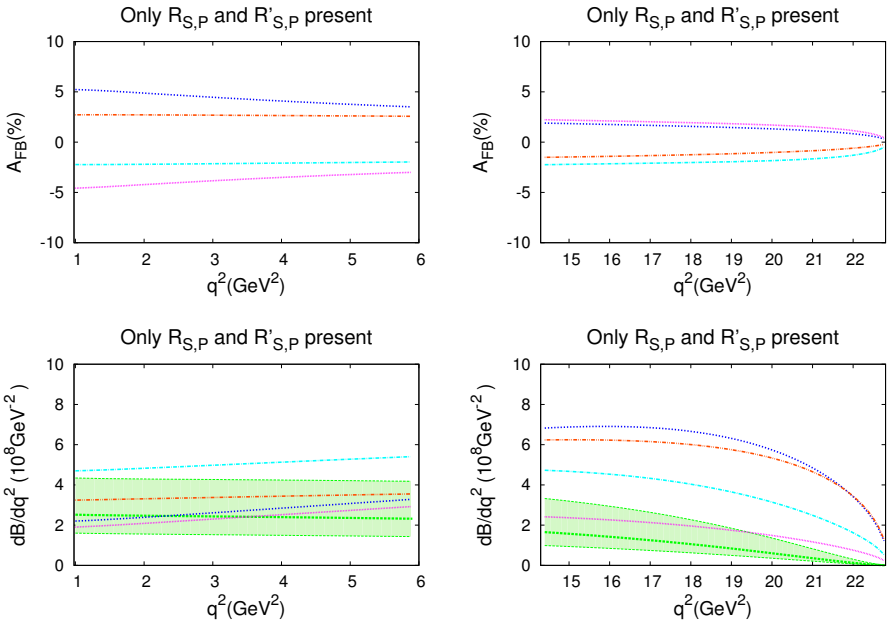

Figure 6. The left (right) panels of the figure show A_{FB} and DBR for $\bar{B}_d^0 \to \bar{K}\mu^+\mu^-$ in the low-q^2 (high-q^2) region, in the scenario where all NP SP couplings are present. The band corresponds to the SM prediction and its uncertainties; the lines show predictions for some representative values of NP parameters (R_S, R_P, R'_S, R'_P) . For example, the blue curves in the low-q^2 and high-q^2 regions correspond to $(-2.50, 6.18, -2.84, -5.64)$ and $(-2.41, 1.86, -2.07, 1.42)$, respectively.

zero crossing. The DBR also is significantly affected only if both the primed and unprimed SP couplings are present: it can be enhanced by up to a factor of 3.

New T couplings are also expected to give rise to A_{FB} through the $Y'_{VA\text{-}T}$ terms in eq. (C.12). It is observed from figure 7 that $A_{FB}(q^2)$ can be enhanced up to 5-6% in almost the entire q^2 region. Moreover, at $q^2 \gtrsim 21\,\text{GeV}^2$, the peak value of $A_{FB}(q^2)$ reaches a larger value ($\sim 30\%$). The value of $A_{FB}(q^2)$ is always positive or always negative, i.e. there is no zero crossing point. The DBR values do not go significantly outside the SM-allowed range.

When VA and T couplings are present simultaneously, a DBR enhancement of up to a factor of 2 is possible, while A_{FB} can be large only at extremely high q^2. On the other hand, when SP and T couplings are present simultaneously, their interference can have a large impact on A_{FB}. The interference term $Y'_{SP\text{-}T}$ that contributes to A_{FB} is not suppressed by m_μ/m_b, and therefore a large A_{FB} is possible, as can be seen from figure 8. This is also the only combination of NP couplings where a zero crossing may occur. Among the asymmetries considered in this paper, this is the one where the SP and T operators can have the largest impact. The DBR can also be enhanced by up to a factor of 2-3 at large q^2 due to the simultaneous presence of primed and unprimed SP operators.

7 $\bar{B}_d^0 \to \bar{K}^*\mu^+\mu^-$

The measurement of the forward-backward asymmetry in $\bar{B}_d^0 \to \bar{K}^*\mu^+\mu^-$ by the Belle collaboration [10, 11], which showed a deviation from the SM prediction, indicates the

JHEP11(2011)121

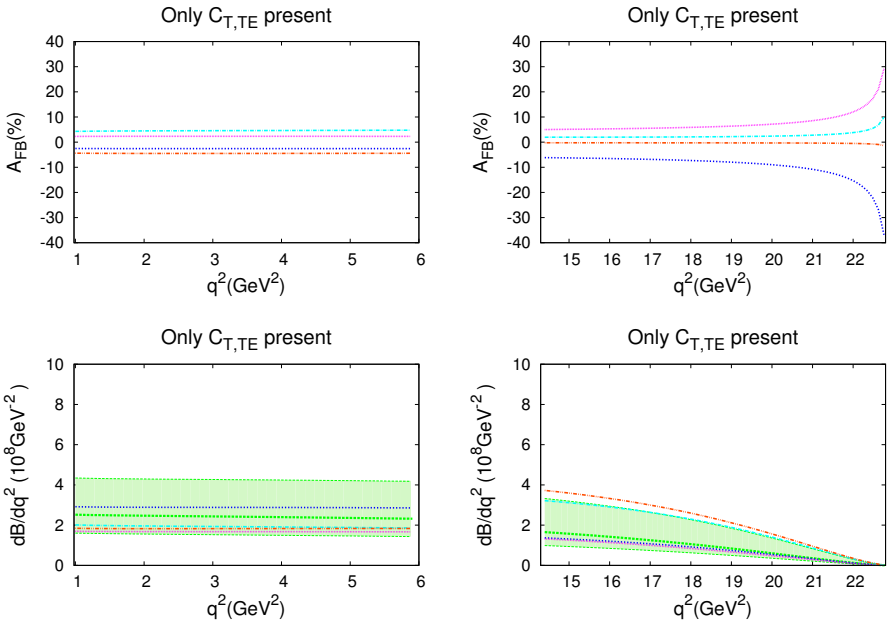

Figure 7. The left (right) panels of the figure show A_{FB} and DBR for $\bar{B}_d^0 \to \bar{K}\mu^+\mu^-$ in the low-q^2 (high-q^2) region, in the scenario where only T terms are present. The band corresponds to the SM prediction and its uncertainties; the lines show predictions for some representative values of NP parameters (C_T, C_{TE}). For example, the blue curves in the low-q^2 and high-q^2 regions correspond to $(0.30, 0.37)$ and $(0.49, 0.57)$, respectively.

possibility of the presence of new physics. According to the SM, A_{FB} is $\leq 20\%$ and negative at low q^2, has a zero crossing at $q^2 \approx 4\,\mathrm{GeV}^2$, and is positive but $\leq 40\%$ for larger q^2 values. The experiment showed the asymmetry to be positive throughout the range of q^2 — consequently no zero crossing — and $A_{FB} \approx 60\%$ at large q^2 values. This has generated a special interest in this decay.

There have already been a number of theoretical studies, both within the SM [52, 53, 60] and in specific NP scenarios [57, 58, 61, 62], focusing on the branching fraction and A_{FB} of $\bar{B}_d^0 \to \bar{K}^*\mu^+\mu^-$. For example, ref. [59] has pointed out that $A_{FB}(q^2)$ is a sensitive probe of NP that affects the SM Wilson coefficients. Other observables based on the K^* spin amplitudes of this decay are at present under active theoretical and experimental analysis [57, 58, 60]. Finally, more challenging observables, such as the polarized lepton forward-backward asymmetry [46, 47, 55, 56], have also been considered, though the measurement of this quantity is still lacking.

In the coming years, the LHCb experiment will collect around 3000 events of $\bar{B}_d^0 \to \bar{K}^*\mu^+\mu^-$ per fb^{-1} in the full range of q^2. An integrated luminosity of $2\,\mathrm{fb}^{-1}$ already would allow the extraction of the SM zero of A_{FB} (if it is there) with a precision of $\pm 0.5\,\mathrm{GeV}^2$ [87]. Indeed, a dataset of $100\,\mathrm{pb}^{-1}$ would already improve the world precision obtained by Babar, Belle and CDF. These measurements would also permit many of the additional tests for NP mentioned above.

The decay $\bar{B}_d^0 \to \bar{K}^*\mu^+\mu^-$, with $\bar{K}^*$ decaying to $\bar{K}\pi$, has four particles in the final state.

JHEP11(2011)121

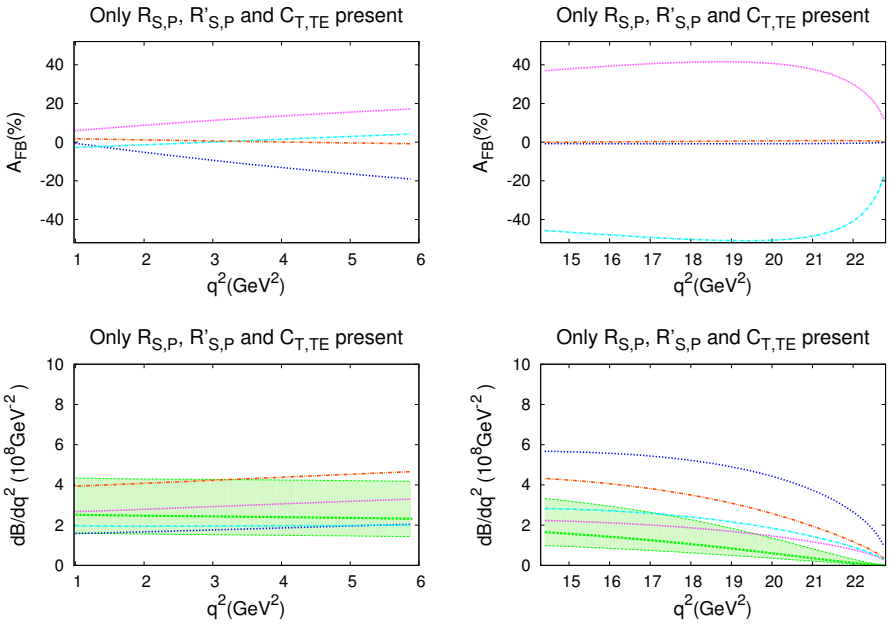

Figure 8. The left (right) panels of the figure show A_{FB} and DBR for $\bar{B}_d^0 \to \bar{K}\mu^+\mu^-$ in the low-q^2 (high-q^2) region, in the scenario where both SP and T terms are present. The band corresponds to the SM prediction and its uncertainties; the lines show predictions for some representative values of NP parameters $(R_S, R_P, R'_S, R'_P, C_T, C_{TE})$. For example, the magenta curves in the low-q^2 and high-q^2 regions correspond to $(-0.09, -2.24, 0.16, -2.14, -0.33, -0.40)$ and $(-0.40, 1.87, -0.59, 1.88, -0.34, 0.66)$, respectively.

This implies that there are three physical angles that can specify the relative directions of these four final-state particles. The differential decay rate as a function of these three angles has much more information than just the forward-backward asymmetry. Indeed, A_{FB} is just one of the observables that can be derived from the complete angular analysis of this decay. In this section we also consider other CP-conserving observables.

7.1 Angular analysis

The complete angular distribution in $\bar{B}_d^0 \to \bar{K}^*\mu^+\mu^-$ has been calculated in refs. [88, 89] within the SM. In this section, we calculate the angular distribution in the presence of NP, which is a new result. The full transition amplitude for $\bar{B}(p_B) \to \bar{K}^*(p_{K^*}, \epsilon^*)\mu^+(p_\mu^+)\mu^-(p_\mu^-)$ is

$$i\mathcal{M}(\bar{B}_d^0 \to \bar{K}^*\mu^+\mu^-) = (-i)\frac{1}{2}\left[\frac{4\,G_F}{\sqrt{2}}\frac{\alpha_{em}}{4\pi}(V_{ts}^*V_{tb})\right] \times \left[M_{V\mu}L^\mu + M_{A\mu}L^{\mu 5} + M_S L + M_P L^5 + M_{T\mu\nu}L^{\mu\nu} + iM_{E\mu\nu}L_{\alpha\beta}\epsilon^{\mu\nu\alpha\beta}\right], \tag{7.1}$$

where the L's are defined in eq. (2.8). The M's are given in appendix D.

The complete three-angle distribution for the decay $\bar{B} \to \bar{K}^*(\to \bar{K}\pi)\mu^+\mu^-$ can be expressed in terms of q^2, two polar angles θ_μ, θ_K, and the angle between the planes of

JHEP11(2011)121

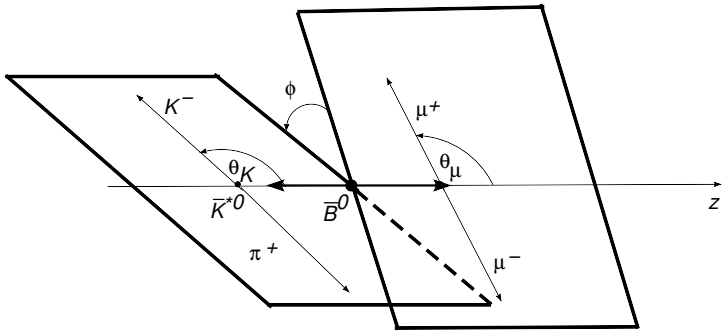

Figure 9. The description of the angles $\theta_{\mu,K}$ and ϕ in the angular distribution of $\bar{B} \to \bar{K}^*(\to \bar{K}\pi)\mu^+\mu^-$ decay.

the dimuon and $K\pi$ decays, ϕ. These angles are described in figure 9. We choose the momentum and polarization four-vectors of the K^* meson in the dimuon rest frame as

$$\begin{aligned} p_{K^*} &= (E_{K^*}, 0, 0, |\vec{p}_{K^*}|) \ , \\ \varepsilon(0) &= \frac{1}{m_{K^*}}(|\vec{p}_{K^*}|, 0, 0, E_{K^*}) \ , \quad \varepsilon(\lambda = \pm 1) = \mp\frac{1}{\sqrt{2}}(0, 1, \pm i, 0) \ , \end{aligned} \tag{7.2}$$

with

$$E_{K^*} = \frac{m_B^2 - m_{K^*}^2 - q^2}{2\sqrt{q^2}}, \quad |\vec{p}_{K^*}| = \sqrt{E_{K^*}^2 - m_{K^*}^2} \ . \tag{7.3}$$

The three-angle distribution can be obtained using the helicity formalism:

$$\begin{aligned} \frac{d^4\Gamma}{dq^2 d\cos\theta_\mu d\cos\theta_K d\phi} &= N_F \Big\{ \cos^2\theta_K \Big(I_1^0 + I_2^0 \cos 2\theta_\mu + I_3^0 \cos\theta_\mu \Big) \\ &+ \sin^2\theta_K \Big(I_1^T + I_2^T \cos 2\theta_\mu + I_3^T \cos\theta_\mu \\ &+ I_4^T \sin^2\theta_\mu \cos 2\phi + I_5^T \sin^2\theta_\mu \sin 2\phi \Big) + \sin 2\theta_K \Big(I_1^{LT} \sin 2\theta_\mu \cos\phi \\ &+ I_2^{LT} \sin 2\theta_\mu \sin\phi + I_3^{LT} \sin\theta_\mu \cos\phi + I_4^{LT} \sin\theta_\mu \sin\phi \Big) \Big\} \ , \end{aligned} \tag{7.4}$$

where the normalization factor N_F is

$$N_F = \frac{3\alpha_{em}^2 G_F^2 |V_{ts}^* V_{tb}|^2 |\vec{p}_{K^*}^B| \beta_\mu}{2^{14}\pi^6 m_B^2} Br(K^* \to K\pi) \ . \tag{7.5}$$

Here $\beta_\mu = \sqrt{1 - 4m_\mu^2/q^2}$, and $|\vec{p}_{K^*}^B|$ is the magnitude of the K^* momentum in the B-meson rest frame:

$$|\vec{p}_{K^*}^B| = \frac{1}{2m_B}\sqrt{m_B^4 + m_{K^*}^4 + q^4 - 2[q^2 m_B^2 + m_{K^*}^2(m_B^2 + q^2)]} \ . \tag{7.6}$$

The twelve angular coefficients I depend on the couplings, kinematic variables and form factors, and are given in appendix D. In this paper we concentrate on the CP-conserving

JHEP11(2011)121

observables: the DBR, the forward-backward asymmetry A_{FB}, the polarization fraction f_L, and the asymmetries $A_T^{(2)}$ and A_{LT}.

The theoretical predictions for the relevant $B \to K^*$ form factors are rather uncertain in the region ($7\,\text{GeV}^2 \le q^2 \le 12\,\text{GeV}^2$) due to nearby charmed resonances. The predictions are relatively more robust in the lower and higher q^2 regions. We therefore concentrate on calculating the angular distribution in the low-q^2 ($1\ \text{GeV}^2 \le q^2 \le 6\ \text{GeV}^2$) and the high-$q^2$ ($q^2 \ge 14.4\ \text{GeV}^2$) regions. For numerical calculations, we follow ref. [62] for the form factors: in the low-q^2 region, we use the form factors obtained using QCD factorization, while in the high-q^2 region, we use the form factors calculated in the light-cone sum-rule approach.

7.2 Differential branching ratio and forward-backward asymmetry

The forward-backward asymmetry for the muons is defined by

$$A_{FB}(q^2) = \frac{\int_0^1 d\cos\theta_\mu \frac{d^2\Gamma}{dq^2 d\cos\theta_\mu} - \int_{-1}^0 d\cos\theta_\mu \frac{d^2\Gamma}{dq^2 d\cos\theta_\mu}}{\int_0^1 d\cos\theta_\mu \frac{d^2\Gamma}{dq^2 d\cos\theta_\mu} + \int_{-1}^0 d\cos\theta_\mu \frac{d^2\Gamma}{dq^2 d\cos\theta_\mu}} \,. \tag{7.7}$$

It can be obtained by integrating over the two angles θ_K and ϕ in eq. (7.4). We obtain the double differential decay rate as

$$\frac{d^2\Gamma}{dq^2 d\cos\theta_\mu} = \frac{8\pi N_F}{3}\left[\frac{1}{2}\left(I_1^0 + I_2^0\cos 2\theta_\mu + I_3^0\cos\theta_\mu\right) + \left(I_1^T + I_2^T\cos 2\theta_\mu + I_3^T\cos\theta_\mu\right)\right] \tag{7.8}$$

Further integration over the angle θ_μ gives the differential decay rate. The contribution of the NP operators to the differential branching ratio and forward-backward asymmetry of $\bar{B}_d^0 \to \bar{K}^*\mu^+\mu^-$ was examined in detail in ref. [62]. We do not reproduce the analysis here, but only give the results below.

If only $R_{V,A}$ couplings are present, A_{FB} can be enhanced at low q^2, while keeping it positive, so that there is no zero crossing as indicated by the recent data [10, 11, 13, 14]. However, an enhancement at high q^2, also indicated by the same data, is not possible. On the other hand, if only $R'_{V,A}$ couplings are present, A_{FB} can become large and positive at high q^2, but then it has to be large and negative at low q^2. These couplings are therefore unable to explain the positive values of A_{FB} at low q^2. Thus, in order to reproduce the current $\bar{B}_d^0 \to \bar{K}^*\mu^+\mu^-$ experimental data, one needs both unprimed and primed NP VA operators. The NP coupling values that come closest to the data typically correspond to suppressed DBR at low q^2. (See figure 10.) But it is also possible to have a large A_{FB} (up to 60%) in the entire q^2 region while being consistent with the SM prediction for the DBR. At present, the errors on the measurements are quite large. However, if future experiments reproduce the current central values with greater precision, this will put important constraints on any NP proposed to explain the data.

New SP couplings by themselves cannot significantly affect either the DBR or the A_{FB} predictions of the SM. New T couplings in general tend to enhance DBR significantly, by up to a factor of 2, while not contributing any additional terms to the asymmetry. As a result, the magnitude of A_{FB} is suppressed. The zero crossing can be anywhere in the entire q^2 range, or it may disappear altogether. However, whenever it is present, it is always a SM-like (positive) crossing. When SP and T couplings are present simultaneously, additional

JHEP11(2011)121

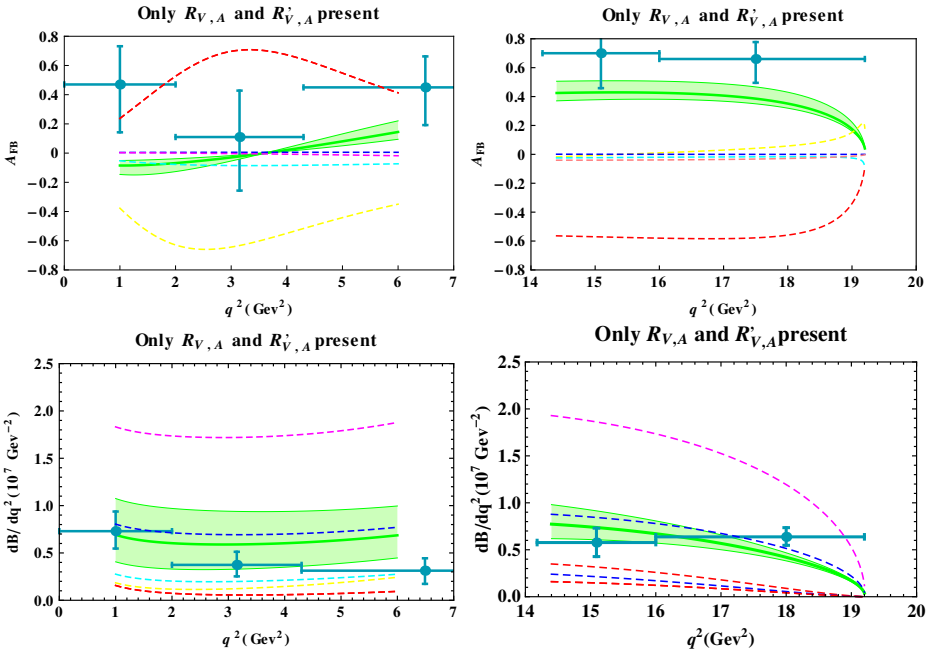

Figure 10. The left (right) panels of the figure show A_{FB} and DBR for $\bar{B}^0_d \to \bar{K}^*\mu^+\mu^-$ in the low-q^2 (high-q^2) region, in the scenario where both (R_V, R_A) and (R'_V, R'_A) terms are present. The band corresponds to the SM prediction and its uncertainties; the lines show predictions for some representative values of NP parameters (R_V, R_A, R'_V, R'_A). For example, the red curves for A_{FB} in the low and high q^2 regions correspond to $(-1.55, 1.75, 6.16, 1.73)$ and $(-5.79, 1.10, 0.47, -3.34)$, respectively. The pink curves for DBR in the low-q^2 and high-q^2 regions correspond to $(1.96, -4.09, 4.61, 0.13)$. For comparison, the experimental data are also displayed in blue cross lines.

contributions to A_{FB} that are not suppressed by m_μ/m_B are possible. As a result, A_{FB} obtained with this combination can be marginally enhanced as compared to the case with only T operators. It is then possible to have no zero crossing. However, the magnitude of A_{FB} cannot be large in the high-q^2 region.

7.3 Polarization fraction f_L

The differential decay rate and K^* polarization fractions can be found by integrating over the three angles in eq. (7.4) to get

$$\frac{d\Gamma}{dq^2} = \frac{8\pi N_F}{3}(A_L + A_T)\,, \tag{7.9}$$

where the longitudinal and transverse polarization amplitudes A_L and A_T are obtained from eq. (7.8):

$$A_L = \left(I_1^0 - \frac{1}{3}I_2^0\right), \quad A_T = 2\left(I_1^T - \frac{1}{3}I_2^T\right)\,. \tag{7.10}$$

It can be seen from the expressions for the I's in appendix D [see eq. (D.15)] that SP couplings cannot affect A_T. The longitudinal and transverse polarization fractions, f_L and

JHEP11(2011)121

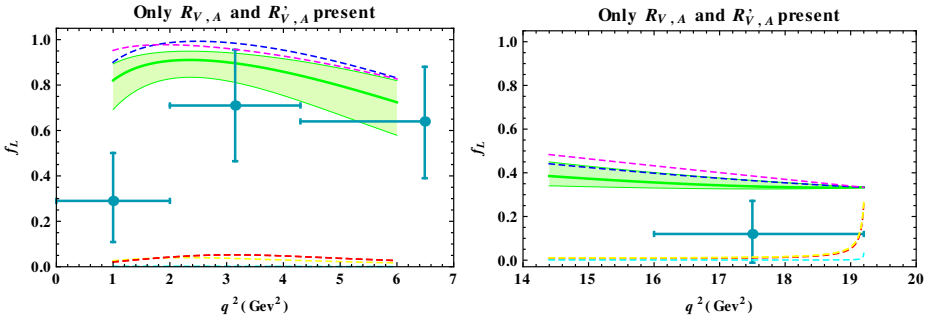

Figure 11. The left (right) panel of the figure shows f_L for $\bar{B}^0_d \to \bar{K}^* \mu^+ \mu^-$ in the low-q^2 (high-q^2) region, in the scenario where both (R_V, R_A) and (R'_V, R'_A) terms are present. For example, the blue curves in the low-q^2 and high-q^2 regions correspond to $(1.64, -0.90, 4.27, -0.91)$ and $(1.96, -4.09, 4.61, 0.13)$, respectively. For comparison, the experimental data are also displayed in blue cross lines.

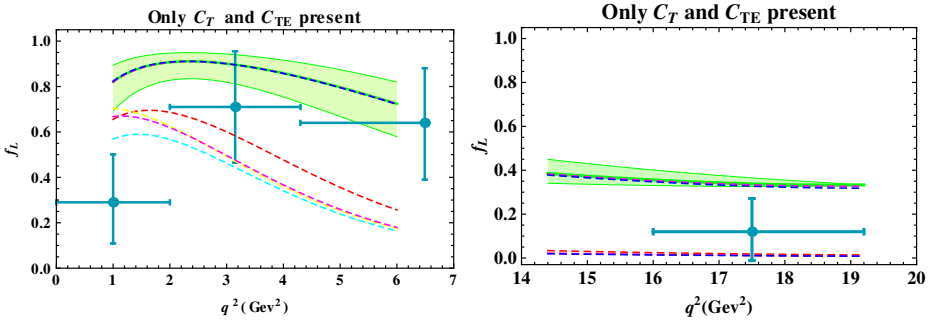

Figure 12. The left (right) panel of the figure shows f_L for $\bar{B}^0_d \to \bar{K}^* \mu^+ \mu^-$ in the low-q^2 (high-q^2) region, in the scenario where only new T couplings are present. The band corresponds to the SM prediction and its uncertainties; the lines show predictions for some representative values of NP parameters (C_T, C_{TE}). For example, the red curves in the low-q^2 and high-q^2 regions correspond to $(0.66, -0.14)$ and $(0.3, -0.46)$, respectively.

f_T, respectively, are defined as

$$f_L = \frac{A_L}{A_L + A_T} \ , \qquad f_T = \frac{A_T}{A_L + A_T} \ . \tag{7.11}$$

In the SM, f_L can be as large as 0.9 at low q^2, and it decreases to about 0.3 at high q^2. As can be seen from figure 11, new VA couplings can suppress f_L substantially: it can almost vanish in some allowed parameter range.

New SP couplings cannot change the value of f_L outside the range allowed by the SM. This may be attributed to the strong constraints on the values of these couplings. New T couplings tend to suppress f_L, except at $q^2 \approx$ 1-2 GeV^2, where the value of f_L cannot be less than 0.5 as may be seen from figure 12. Since both VA and T couplings tend to suppress f_L, their combined effect results in a similar behavior.

JHEP11(2011)121

7.4 Angular asymmetries $A_T^{(2)}$ and A_{LT}

In this subsection we consider the two angular asymmetries $A_T^{(2)}$ and A_{LT}. The first quantity was discussed before in ref. [57], while A_{LT} is introduced here for the first time.

The CP-conserving transverse asymmetry $A_T^{(2)}$ can be defined through the double differential decay rate

$$\frac{d^2\Gamma}{dq^2 d\phi} = \frac{1}{2\pi}\frac{d\Gamma}{dq^2}\Big[1 + f_T\left(A_T^{(2)}\cos 2\phi + A_T^{(im)}\sin 2\phi\right)\Big] . \tag{7.12}$$

Here $A_T^{(im)}$ depends on the imaginary part of a certain combination of amplitudes and can be used to construct CP-violating observables. We will not consider it any further in this work. The asymmetry $A_T^{(2)}$ can be obtained by integrating over the two polar angles θ_μ and θ_K in eq. (7.4). It can be expressed as

$$A_T^{(2)} = \frac{4I_4^T}{3A_T}. \tag{7.13}$$

We observe that $A_T^{(2)}$ cannot be affected by SP couplings.

In the SM,

$$A_T^{(2)} \approx \frac{4\beta_\mu^2\left(|A_\perp^V|^2 - |A_\parallel^V|^2 + |A_\perp^A|^2 - |A_\parallel^A|^2\right)}{3A_T} . \tag{7.14}$$

The transversity amplitudes $A_{\parallel,\perp}$ are defined through eqs. (D.11) and (D.12) given in appendix D. At leading order in Λ_{QCD}/E_{K^*}, Λ_{QCD}/m_b and α_s (the LEET limit), one can use the form-factor relations of refs. [50, 51] and neglect terms of $\mathcal{O}(m_{K^*}^2/m_B^2)$ to obtain

$$A_V^+ \approx 0 \ , \quad A_A^+ \approx 0 . \tag{7.15}$$

Thus, in the low-q^2 region,

$$A_\parallel^i \approx \frac{A_i^-}{\sqrt{2}} \ , \quad A_\perp^i \approx -\frac{A_i^-}{\sqrt{2}} \quad \text{for} \quad i = V, A , \tag{7.16}$$

which corresponds to the LEET limit. $A_T^{(2)} \approx 0$ in the SM and is independent of form factors up to corrections of order Λ_{QCD}/E_{K^*}, Λ_{QCD}/m_b and α_s, i.e. the hadronic uncertainty is small. This can be seen in figures 13 and 14. This indicates that corrections to the LEET limit are small, and makes $A_T^{(2)}$ an excellent observable to look for new-physics effects [57].

We now examine the longitudinal-transverse asymmetry A_{LT}, defined by

$$A_{LT} = \frac{\int_{-\pi/2}^{\pi/2} d\phi (\int_0^1 d\cos\theta_K \frac{d^3\Gamma}{dq^2 d\phi d\cos\theta_K} - \int_{-1}^0 d\cos\theta_K \frac{d^3\Gamma}{dq^2 d\phi d\cos\theta_K})}{\int_{-\pi/2}^{\pi/2} d\phi (\int_0^1 d\cos\theta_K \frac{d^3\Gamma}{dq^2 d\phi d\cos\theta_K} + \int_{-1}^0 d\cos\theta_K \frac{d^3\Gamma}{dq^2 d\phi d\cos\theta_K})} . \tag{7.17}$$

One can compare A_{LT} to A_{FB}. In A_{FB} the angle ϕ is integrated over its entire range, while in A_{LT} ϕ is only integrated over the range $(-\pi/2, \pi/2)$. This choice of integration range eliminates all terms which depend on the imaginary part of combinations of amplitudes in

JHEP11(2011)121

the angular distribution. (These eliminated terms can be used to construct CP-violating observables and will not be discussed here.) In A_{LT} only the CP-conserving parts of the angular distribution survive. Note that, in the CP-conserving limit, A_{LT} is the same as the observable S_5 defined in ref. [61], apart from a normalization constant. The quantity A_{LT} can also be expressed in terms of the observables $A_T^{(3)}$ and $A_T^{(4)}$ defined in ref. [60]. However, A_{LT} is easily extracted from the angular distribution and has different properties in the LEET limit than $A_T^{(3)}$ and $A_T^{(4)}$.

Using eq. (7.4), the asymmetry A_{LT} can be expressed as

$$A_{LT} = \frac{I_3^{LT}}{2(A_L + A_T)}. \tag{7.18}$$

We observe from eq. (D.16) that A_{LT} depends on the VA couplings, as well as on V-S, S-TE, and P-T interference terms. In the SM,

$$A_{LT} = \frac{\beta_\mu \mathrm{Re}[A^L_{0,VA}(A^{V*}_\perp - A^{A*}_\perp) - A^R_{0,VA}(A^{V*}_\perp + A^{A*}_\perp)]}{\sqrt{2}(A_L + A_T)} \,. \tag{7.19}$$

Now, in the LEET limit, $A^+_{V,A} \approx 0$. Hence, in this limit,

$$A_{LT}^{LEET} \propto \frac{\mathrm{Re}[A^0_V A^{-*}_A + A^0_A A^{-*}_V]}{A_L + A_T} \,. \tag{7.20}$$

From this it can be shown that the SM predicts $A_{LT} = 0$ at

$$q^2 \approx -\frac{C_7^{\mathrm{eff}} m_b m_B^2}{C_7^{\mathrm{eff}} m_b + C_9^{\mathrm{eff}} m_B} \approx 1.96 \text{ GeV}^2 \,. \tag{7.21}$$

Thus, just like A_{FB}, the quantity A_{LT} also has a zero crossing which is independent of form factors in the LEET limit. Note that the zero crossing of A_{LT} is different from that of A_{FB}. Figures 13 and 14 also demonstrate that the zero crossing of A_{LT} has a very small hadronic uncertainty. This indicates small corrections to the LEET limit, making the position of the zero crossing of A_{LT} a robust prediction of the SM. This quantity would therefore be very useful in searching for new-physics effects.

New VA couplings can affect $A_T^{(2)}$ significantly: they can enhance its magnitude by a large amount, change its sign, and change its q^2-dependence. The zero-crossing point may be at a value of q^2 different from that predicted by the SM.

Since A_{LT} here is identical to the observable S_5 in refs. [61, 67] in the CP-conserving limit (apart from a normalization factor), the zero-crossing in both of these observables is expected to take place at the same q^2. Indeed, the results agree at LO, while the NLO corrections can shift the q^2 at the zero-crossing to $q^2 = 2.24^{+0.06}_{-0.08}$ [61]. Note that the deviation due to new VA couplings can be much larger than the effects due to NLO corrections.

Except at very low q^2, the magnitude of A_{LT} is generally suppressed by new VA couplings. The primed VA couplings can be constrained by A_{LT} better than the unprimed VA couplings. In both cases, the value of A_{LT} can be anywhere in the q^2 range, and can be positive or negative. In particular, there may or may not be a zero crossing, and if there is, its position can be different from that of the SM.

JHEP11(2011)121

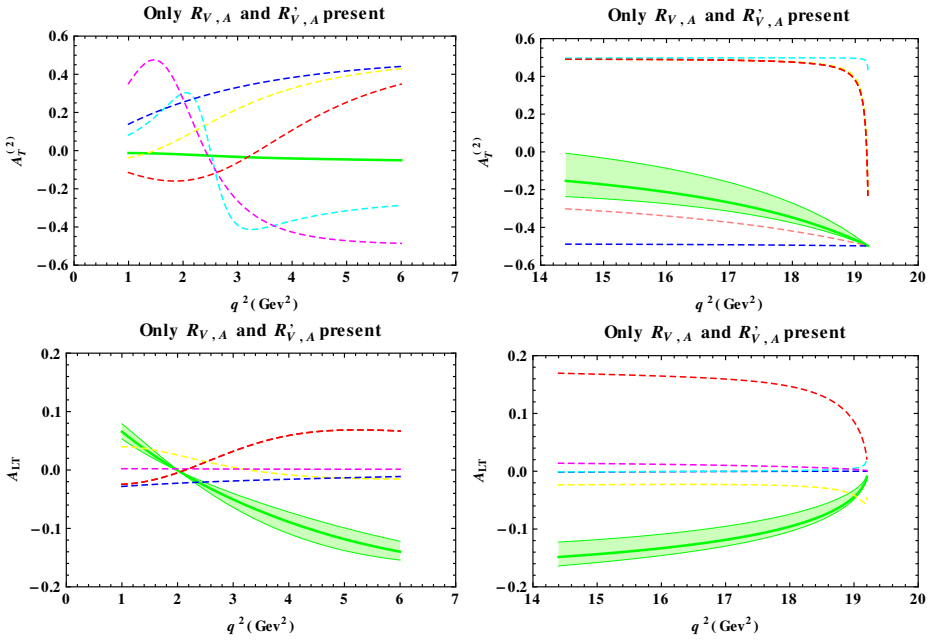

Figure 13. The left (right) panels of the figure show $A_T^{(2)}$ and A_{LT} for $\bar{B}_d^0 \to \bar{K}^*\mu^+\mu^-$ in the low-q^2 (high-q^2) region, in the scenario where both (R_V, R_A) and (R'_V, R'_A) terms are present. The band corresponds to the SM prediction and its uncertainties; the lines show predictions for some representative values of NP parameters (R_V, R_A, R'_V, R'_A). For example, the pink curves for $A_T^{(2)}$ in the low-q^2 and high-q^2 regions correspond to $(1.96, -4.09, 4.61, 0.13)$ and $(1.64, -0.90, 4.27, -0.91)$, respectively. The red curves for A_{LT} in the low-q^2 and high-q^2 regions correspond to $(-1.55, 1.75, 6.16, 1.73)$ and $(-5.79, 1.10, 0.47, -3.33)$, respectively.

New SP couplings do not affect $A_T^{(2)}$, and A_{LT} qualitatively behaves similarly to the SM. New T couplings in general tend to suppress the magnitudes of both asymmetries (see figure 14).

8 Discussion and summary

Flavor-changing neutral current (FCNC) processes are expected to be incisive probes of new physics. In the SM, they occur only at loop level, and hence are suppressed. This may allow the new-physics (NP) effects to be identifiable. Of course, since we have no clue about what form the NP takes, the observations from a variety of processes are necessary. In this paper, we have focussed on the processes that involve the effective transition $b \to s\mu^+\mu^-$.

The transition $b \to s\mu^+\mu^-$ is responsible for many decay modes such as $\bar{B}_s^0 \to \mu^+\mu^-$, $\bar{B}_d^0 \to X_s\mu^+\mu^-$, $\bar{B}_s^0 \to \mu^+\mu^-\gamma$, $\bar{B}_d^0 \to \bar{K}\mu^+\mu^-$, $\bar{B}_d^0 \to \bar{K}^*\mu^+\mu^-$. While some of these processes (e.g. $\bar{B}_s^0 \to \mu^+\mu^-$) have not yet been observed, the upper bounds on their branching ratios have already yielded strong constraints on NP. Some of these processes have been observed and the measurements of their branching fractions, as well as of additional observables such as the forward-backward asymmetries, are available. Indeed, the recently-observed muon forward-backward asymmetry in $\bar{B}_d^0 \to \bar{K}^*\mu^+\mu^-$ has been found to deviate slightly from the SM predictions. If this is in fact due to the presence of NP, such NP

JHEP11(2011)121

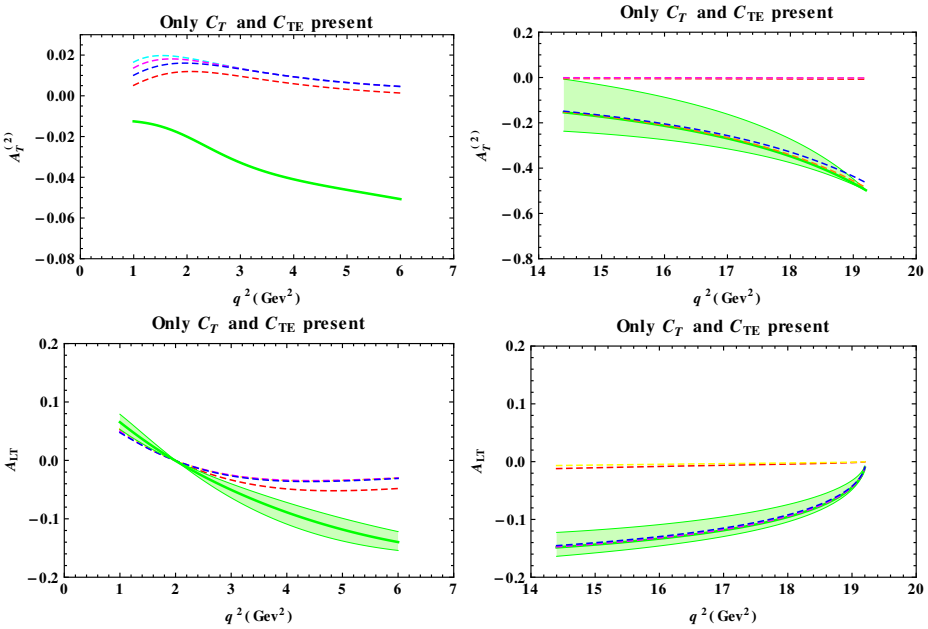

Figure 14. The left (right) panels of the figure show $A_T^{(2)}$ and A_{LT} for $\bar{B}_d^0 \to \bar{K}^* \mu^+ \mu^-$ in the low-q^2 (high-q^2) region, in the scenario where only new T couplings are present. The band corresponds to the SM prediction and its uncertainties; the lines show predictions for some representative values of NP parameters (C_T, C_{TE}). For example, the blue curves for $A_T^{(2)}$ in the low-q^2 and high-q^2 regions correspond to $(0.3, -0.46)$ and $(-0.005, 0.014)$, respectively. The red curves for A_{LT} in the low-q^2 and high-q^2 regions correspond to $(0.3, -0.46)$ and $(0.66, -0.14)$, respectively.

should contribute to all the other decays involving the effective transition $b \to s\mu^+\mu^-$. The effects of this NP on these decay modes would be correlated, and hence a combined analysis of all these decay modes would be invaluable in discerning the type of NP present.

While specific models of NP may be used and their effect on the relevant observables studied, we have chosen to explore the NP in a model-independent way, in terms of the Lorentz structures of the NP operators that contribute to the effective $b \to s\mu^+\mu^-$ Hamiltonian. We have performed a general analysis that includes NP vector-axial vector (VA), scalar-pseudoscalar (SP), and/or tensor (T) operators. We have computed the effects of such NP operators, individually and in all combinations, on these decays. We have taken the couplings to be real and have considered the CP-conserving observables in this paper; the CP-violating observables are discussed in ref. [72]. The aim is to find NP signals, and using them, to identify the Lorentz structure of the NP. As the first step towards this goal, we calculate the constraints on the NP couplings, and, keeping the couplings within these bounds, we look for the observables where the NP signal can potentially stand out above the SM background.

It is crucial to understand this SM background, which makes it imperative to use observables whose values are predicted reasonably accurately within the SM. The main source of the SM uncertainties is the hadronic matrix elements, whose theoretical calculations often have errors of the order of tens of percent. We have handled this on many levels.

JHEP11(2011)121

First, we have tried to identify observables that will not be very sensitive to the hadronic uncertainties. For example in $\bar{B}_d^0 \to \bar{K}\mu^+\mu^-$, the SM prediction for the forward-backward asymmetry is simply zero, independent of any hadronic elements. Also, while the differential branching ratios may be strongly dependent on the hadronic matrix elements, the forward-backward asymmetries are less so. Furthermore, the large-energy effective theory (LEET) limits can be used to control the uncertainties in the low-q^2 region for observables like A_{FB} and $A_T^{(2)}$. For example, certain observables, such as the zero-crossing of A_{FB} in $\bar{B}_d^0 \to \bar{K}^*\mu^+\mu^-$, can be shown to be robust under form-factor uncertainties in the LEET limit. The longitudinal-transverse asymmetry A_{LT} in $\bar{B}_d^0 \to \bar{K}^*\mu^+\mu^-$ also has a zero crossing in the SM with small hadronic uncertainties. These measurements can even be used to extract the parameters of the NP operators, to a very good approximation.

Also, we focus only on the situations where the NP contribution can be so significant that it will stand out even if the SM errors were magnified. Our figures show bands for SM predictions that include the form-factor uncertainties as quoted in the form-factor calculations, and these are overlaid with some examples of the allowed values of these observables when NP contributions are included. This allows the scaling of these uncertainties to be easily visualized. We identify and emphasize only those situations where the results with the NP can be significantly different from those without the NP, even if the hadronic uncertainties were actually much larger. Note that further inclusion of the NLO QCD corrections would affect the central values of the SM predictions to a small extent, while also decreasing the renormalization scale uncertainty. However, since our primary interest is looking for observables where the NP effects are large, a LO analysis is sufficient.

Our results are summarized in table 1, for the cases where the NP has only one type of Lorentz structure: VA, SP or T. We note certain generic features of the influence of different NP Lorentz structures.

New VA operators are the ones that influence the observables strongly in most cases. They typically can interfere with the SM terms constructively or destructively, thus enhancing or suppressing the differential branching ratios by up to factors of 2 or 3. They also are able to enhance almost all the asymmetries, the notable exception being A_{FB} in $\bar{B}_d^0 \to \bar{K}\mu^+\mu^-$, where the VA operators cannot contribute. But for most other observables, this kind of NP can potentially be observed. This can be traced to the large magnitudes of the NP couplings still allowed by data, which in turn can be traced to the possibility of interference between the new VA operators with the SM operators that allows more freedom for the new VA couplings. Typically, the $R_{V,A}$ couplings are constrained more weakly than the $R'_{V,A}$ couplings, since the corresponding operators have the same structure as those of the SM, allowing strong destructive interferences. Consequently, the operators with $R_{V,A}$ couplings are more likely to show themselves over and above the SM background. We point out that the exception to this rule is the A_{FB} in $\bar{B}_d^0 \to \bar{K}^*\mu^+\mu^-$ at large q^2, where the $R'_{V,A}$ couplings can cause a larger enhancement.

The SP operators, on the other hand, are handicapped by the stringent constraints from the upper bound on $B(\bar{B}_s^0 \to \mu^+\mu^-)$. If only $R_{S,P}$ or $R'_{S,P}$ couplings are present, the constraints become even more severe. It is for this reason that, even when the SP contributions are unsuppressed by m_μ/m_b, they are not often large enough to stand apart from the SM background.

JHEP11(2011)121

Observable	SM	Only new VA	Only new SP	Only new T
$\bar{B}_s^0 \to \mu^+\mu^-$				
BR	$(3.35 \pm 0.32) \times 10^{-9}$	• Marginal E • Significant S	• Large E • Maximal S	No effect
$\bar{B}_d^0 \to X_s\mu^+\mu^-$				
DBR		• E ($\times 2$) • S ($\div 2$)	• Marginal E	• E ($\times 2$)
A_{FB}	ZC$\approx 3.5\,\mathrm{GeV}^2$	• E(30%) low q^2 • ZC shift / disappearence	• Marginal S	• Marginal S
f_L	• $0.9 \to 0.3$ (low$\to$high q^2)	• Large S at low q^2	• Marginal S	• Marginal E
$\bar{B}_s^0 \to \mu^+\mu^-\gamma$				
DBR		• E ($\times 2 - \times 3$) • S (low q^2)	No effect	• E ($\times 3$)
A_{FB}	ZC$\approx 4.3\,\mathrm{GeV}^2$	• ZC shift / disappearence	No effect	• Large S
$\bar{B}_d^0 \to \bar{K}\mu^+\mu^-$				
DBR		• E ($\times 2$) • Marginal S	• E at high q^2	• Small effect
A_{FB}	Vanishes	• No effect	• E at low q^2 • No ZC	• E at high q^2 • No ZC
$\bar{B}_d^0 \to \bar{K}^*\mu^+\mu^-$				
DBR		• E ($\times 2$) • S ($\div 2$)	No effect	• E ($\times 2$)
A_{FB}	ZC$\approx 3.9\,\mathrm{GeV}^2$	• E at low q^2 • ZC shift / disappearence	No effect	• Significant S • ZC shift
f_L	• $0.9 \to 0.3$ (low$\to$high q^2)	• Large S	No effect	• Significant S
$A_T^{(2)}$	• $\uparrow$ with q^2 • No ZC	• E ($\times 2$) • ZC possible	No effect	• Significant S
A_{LT}	• ZC at low q^2 • more -ve at large q^2	• Significant S • ZC shift / disappearence	No effect	• Significant S

Table 1. The effect of NP couplings on observables. E($\times n$): enhancement by up to a factor of n, S($\div n$): suppression by up to a factor of n, ZC: zero crossing.

The couplings of the T operators, viz. C_T and C_{TE}, are not as suppressed as those of the SP operators. Therefore, they typically contribute significantly to the DBRs. However, the interference terms of these operators with the SM operators often suffer from the m_μ/m_b helicity suppression, and hence they tend to suppress the magnitudes of the asymmetries.

The combination of multiple Lorentz structures in general gives rise to the combination of features of the individual Lorentz structures involved. In particular, if the VA operators appear in conjunction with another Lorentz structure, the effects of the VA operators typically dominate. The T operators can interfere with the SP operators without the

JHEP11(2011)121

m_μ/m_b helicity suppression, but the strong constraints on the SP operators hold them back. A remarkable exception is the combination of SP and T operators in the forward-backward asymmetry in $\bar{B}^0_d \to \bar{K}\mu^+\mu^-$. This asymmetry, which vanishes in the SM, can be enhanced to $\sim 5\%$ at low q^2 with only SP operators, and can be enhanced to $\sim 30\%$ with T operators but only at $q^2 \approx m_B^2$. However, the presence of both SP and T operators allows the asymmetry to be $\sim 40\%$ in the whole high-q^2 region. A similar feature, though to a less-spectacular extent, is observed in A_{FB} of $\bar{B}^0_d \to \bar{K}^*\mu^+\mu^-$ [62].

With the large amount of data expected from the LHC experiments and B-factories in the coming years, we may be able to detect confirmed NP signals in the above processes. In that case, a combined analysis of all these decay modes, as carried out in this paper, would enable us to identify the Lorentz structure of the NP operators. This will be important in establishing precisely what type of NP is present.

Acknowledgments

We thank Gagan Mohanty and Zoltan Ligeti for useful comments, and S. Uma Sankar and Alejandro Szynkman for helpful collaboration on several parts of this analysis. M.D. would like to thank Wolfgang Altmannshofer for useful discussions. This work was financially supported by NSERC of Canada (AKA, DL).

Notes added. After this paper was submitted, the CDF Collaboration reported [90] the measurement of

$$B(\bar{B}^0_s \to \mu^+\mu^-) = (1.8^{+1.1}_{-0.9}) \times 10^{-8} \ . \tag{8.1}$$

On the other hand, the recent LHCb update does not confirm this result [91]. They improve the present upper bound on $B(\bar{B}^0_s \to \mu^+\mu^-)$ to

$$B(\bar{B}^0_s \to \mu^+\mu^-) \leq 1.3 \times 10^{-8} \quad (90\% \text{ C.L.}) \tag{8.2}$$

In addition, LHCb has measured various observables in $\bar{B}^0_d \to \bar{K}^*\mu^+\mu^-$ [92]. Their measurement of the A_{FB} distribution is consistent with the SM prediction, except in the high-q^2 region, where we now see a slight suppression. This is contrary to the measurement of Belle. That is, LHCb does not confirm the Belle result of a large FB asymmetry in the low-q^2 region. Thus, the jury is still out on whether NP has already been seen in these measurements.

A Details of the $\bar{B}^0_d \to X_s\mu^+\mu^-$ analysis

The differential branching ratio for $\bar{B}^0_d \to X_s\mu^+\mu^-$ in SM can be written as

$$\begin{aligned}\left(\frac{\mathrm{d}B}{\mathrm{d}z}\right)_{\rm SM} = B_0 \frac{8}{3}(1-z)^2\sqrt{1-\frac{4t^2}{z}} \times \\ \left[(2z+1)\left(\frac{2t^2}{z}+1\right)|C_9^{\rm eff}|^2 + \left(\frac{2(1-4z)t^2}{z}+(2z+1)\right)|C_{10}^{\rm eff}|^2\right. \\ \left. + 4\left(\frac{2}{z}+1\right)\left(\frac{2t^2}{z}+1\right)|C_7^{\rm eff}|^2 + 12\left(\frac{2t^2}{z}+1\right){\rm Re}(C_7^{\rm eff}C_9^{\rm eff*})\right],\end{aligned} \tag{A.1}$$

JHEP11(2011)121

Here $t \equiv m_\mu/m_b^{\rm pole}$ and $z \equiv q^2/(m_b^{\rm pole})^2$. The normalization constant B_0 is [28]

$$B_0 = \frac{3\alpha_{em}^2\, B(\bar{B} \to X_c e\bar{\nu})}{32\pi^2\, f(\hat{m}_c)\, \kappa(\hat{m}_c)} \frac{|V_{tb}V_{ts}^*|^2}{|V_{cb}|^2} \,, \tag{A.2}$$

where $\hat{m}_c \equiv m_c^{\rm pole}/m_b^{\rm pole}$. We use $\hat{m}_c = 0.29 \pm 0.02$ [32], $B(\bar{B} \to X_c e\bar{\nu}) = 0.1061 \pm 0.0017$ [77] and $|V_{tb}V_{ts}^*|/|V_{cb}| = 0.967 \pm 0.009$ [93]. Here $f(\hat{m}_c)$ is the lowest-order (i.e. parton-model) phase-space factor in $B(\bar{B} \to X_c e\bar{\nu})$:

$$f(\hat{m}_c) = 1 - 8\hat{m}_c^2 + 8\hat{m}_c^6 - \hat{m}_c^8 - 24\hat{m}_c^4 \ln \hat{m}_c \,, \tag{A.3}$$

and the function $\kappa(\hat{m}_c)$ includes both the $O(\alpha_s)$ QCD corrections and the leading-order $(1/m_b^2)$ power correction to $B(\bar{B} \to X_c e\bar{\nu})$:

$$\kappa(\hat{m}_c) = 1 - \frac{2\alpha_s(m_b)}{3\pi} g(\hat{m}_c) + \frac{h(\hat{m}_c)}{2m_b^2} \,. \tag{A.4}$$

Here the two functions are

$$\begin{aligned} g(\hat{m}_c) &= \left(\pi^2 - \frac{31}{4}\right)(1-\hat{m}_c)^2 + \frac{3}{2} \,, \\ h(\hat{m}_c) &= \lambda_1 + \frac{\lambda_2}{f(\hat{m}_c)}\left[-9 + 24\hat{m}_c^2 - 72\hat{m}_c^4 + 72\hat{m}_c^6 - 15\hat{m}_c^8 - 72\hat{m}_c^4 \ln \hat{m}_c\right] . \end{aligned} \tag{A.5}$$

After including all the NP interactions, and neglecting terms suppressed by m_μ/m_b and m_s/m_b, the total differential branching ratio $\mathrm{d}B/\mathrm{d}z$ can be written in the form

$$\left(\frac{\mathrm{d}B}{\mathrm{d}z}\right)_{\rm Total} = \left(\frac{\mathrm{d}B}{\mathrm{d}z}\right)_{\rm SM} + B_0\Big[B_{\text{SM-VA}} + B_{VA} + B_{SP} + B_T\Big] \,, \tag{A.6}$$

where

$$B_{\text{SM-}VA} = \frac{16}{3}(1-z)^2(1+2z)\Big[\mathrm{Re}(C_9^{\rm eff} R_V^*) + \mathrm{Re}(C_{10}R_A^*)\Big] + 32b(1-z)^2\mathrm{Re}(C_7^{\rm eff}R_V^*) \,, \tag{A.7}$$

$$B_{VA} = \frac{8}{3}(1-z)^2(1+2z)\Big[|R_V|^2 + |R_A|^2 + |R_V'|^2 + |R_A'|^2\Big] \,, \tag{A.8}$$

$$B_{SP} = 4\,(1-z)^2\, z\Big[|R_S|^2 + |R_P|^2 + |R_S'|^2 + |R_P'|^2\Big] \,, \tag{A.9}$$

$$B_T = \frac{128}{3}(1-z)^2(1+2z)\Big[|C_T|^2 + 4|C_{TE}|^2\Big] \,. \tag{A.10}$$

Note that here we have separated the contribution of the SM VA operators (subscript $SM\text{-}VA$) from that of the NP VA operators (subscript VA), for clarity.

The forward-backward asymmetry in $\bar{B}_d^0 \to X_s\mu^+\mu^-$ is

$$A_{FB}(q^2) = \frac{\int_0^1 d\cos\theta_\mu \frac{d^2B}{dq^2 d\cos\theta_\mu} - \int_{-1}^0 d\cos\theta_\mu \frac{d^2B}{dq^2 d\cos\theta_\mu}}{\int_0^1 d\cos\theta_\mu \frac{d^2B}{dq^2 d\cos\theta_\mu} + \int_{-1}^0 d\cos\theta_\mu \frac{d^2B}{dq^2 d\cos\theta_\mu}} \,, \tag{A.11}$$

where θ_μ is the angle between the μ^+ and the $\bar{B}^0$ in the dimuon center-of-mass frame. We can write A_{FB} in the form

$$A_{FB}(q^2) = \frac{N(z)}{\mathrm{d}B/\mathrm{d}z} \,, \tag{A.12}$$

JHEP11(2011)121

where the numerator is given by

$$N(z) \;=\; B_0\Big[N_{\rm SM} + N_{\text{SM-VA}} + N_{VA} + N_{SP\text{-}T}\Big]\,, \tag{A.13}$$

with

$$N_{\rm SM} = -8\,C_{10}\,(1-z)^2\Big[2C_7^{\rm eff} + z\,{\rm Re}(C_9^{\rm eff})\Big]\,, \tag{A.14}$$

$$N_{\text{SM-}VA} = -8\,(1-z)^2\Big[z\,{\rm Re}\Big(C_{10}R_V^* + C_9^{\rm eff}R_A^*\Big) + 2C_7^{\rm eff}{\rm Re}(R_A^*)\Big]\,, \tag{A.15}$$

$$N_{VA} = -8\,z\,(1-z)^2\Big[{\rm Re}(R_V R_A^*) - {\rm Re}(R'_V R'^*_A)\Big]\,, \tag{A.16}$$

$$\begin{aligned} N_{SP\text{-}T} = -8\,z\,(1-z)^2\Big[&{\rm Re}\Big\{(R_S+R_P)\,(C_T^* - 2C_{TE}^*)\Big\} \\ &+ {\rm Re}\Big\{(R'_S - R'_P)\,(C_T^* + 2C_{TE}^*)\Big\}\Big]\,. \end{aligned} \tag{A.17}$$

The expressions of eqs. (A.7)–(A.17) are in agreement with ref. [30].

The polarization fractions f_L and f_T are defined as

$$f_L = \frac{H_L(z)}{H_L(z)+H_T(z)}\,, \qquad\qquad f_T = \frac{H_T(z)}{H_L(z)+H_T(z)}\,, \tag{A.18}$$

where

$$H_L(z) = H_L^{\rm SM}(z) + H_L^{{\rm SM}-VA}(z) + H_L^{VA}(z) + H_L^{SP}(z) + H_L^{T}(z)\,, \tag{A.19}$$

$$H_T(z) = H_T^{\rm SM}(z) + H_T^{{\rm SM}-VA}(z) + H_T^{VA}(z) + H_T^{SP}(z) + H_T^{T}(z)\,. \tag{A.20}$$

The components of H_L and H_T functions are

$$H_L^{\rm SM}(z) = \frac{8\,B_0}{3}(1-z)^2\Big[\,\Big|C_9^{\rm eff} + 2C_7^{\rm eff}\Big|^2 + |C_{10}|^2\Big]\,, \tag{A.21}$$

$$H_T^{\rm SM}(z) = \frac{16\,B_0}{3}z(1-z)^2\Big[\,\Big|C_9^{\rm eff} + \frac{2}{z}C_7^{\rm eff}\Big|^2 + |C_{10}|^2\Big]\,, \tag{A.22}$$

$$H_L^{\text{SM-}VA}(z) = \frac{16\,B_0}{3}(1-z)^2\Big[{\rm Re}\left(C_9^{\rm eff}\,R_V^* + C_{10}R_A^*\right) + 2{\rm Re}(C_7^{\rm eff}\,R_V^*)\Big]\,, \tag{A.23}$$

$$H_T^{\text{SM-}VA}(z) = \frac{32\,B_0}{3}(1-z)^2\Big[z{\rm Re}\left(C_9^{\rm eff}\,R_V^* + C_{10}R_A^*\right) + 2{\rm Re}(C_7^{\rm eff}\,R_V^*)\Big], \tag{A.24}$$

$$H_L^{VA}(z) = \frac{8\,B_0}{3}(1-z)^2\Big[|R_V|^2 + |R_A|^2 + |R'_V|^2 + |R'_A|^2\Big]\,, \tag{A.25}$$

$$H_T^{VA}(z) = \frac{16\,B_0}{3}z(1-z)^2\Big[|R_V|^2 + |R_A|^2 + |R'_V|^2 + |R'_A|^2\Big]\,, \tag{A.26}$$

$$H_L^{SP}(z) = \frac{4\,B_0}{3}z(1-z)^2\Big[|R_S|^2 + |R_P|^2 + |R'_S|^2 + |R'_P|^2\Big]\,, \tag{A.27}$$

$$H_T^{SP}(z) = \frac{8\,B_0}{3}z(1-z)^2\Big[|R_S|^2 + |R_P|^2 + |R'_S|^2 + |R'_P|^2\Big]\,, \tag{A.28}$$

$$H_L^{T}(z) = \frac{64\,B_0}{3}(2-z)(1-z)^2\Big[|C_T|^2 + 4|C_{TE}|^2\Big]\,, \tag{A.29}$$

$$H_T^{T}(z) = \frac{128\,B_0}{3}z(1-z)^2\Big[|C_T|^2 + 4|C_{TE}|^2\Big]\,. \tag{A.30}$$

JHEP11(2011)121

B Details of the $\bar{B}_s^0 \to \mu^+\mu^-\gamma$ analysis

The transition amplitude for $\bar{B}_s^0 \to \mu^+\mu^-\gamma$ is

$$
\begin{aligned}
i\mathcal{M}(\bar{B}_s^0 \to \mu^+\mu^-\gamma) = (-i)\frac{1}{2}\Big[-\frac{4G_F}{\sqrt{2}}\frac{\alpha_{em}}{4\pi}(V_{ts}^* V_{tb})\Big] \times \\
\Big\{ \langle\gamma(k)|\bar{s}\gamma_\mu b|\bar{B}_s^0(p_B)\rangle \Big[(C_9^{\rm eff} + R_V + R_V')L^\mu + (C_{10} + R_A + R_A')L^{\mu 5}\Big] \\
+ \langle\gamma(k)|\bar{s}\gamma_\mu\gamma_5 b|\bar{B}_s^0(p_B)\rangle \Big[-(C_9^{\rm eff} + R_V - R_V')L^\mu - (C_{10} + R_A - R_A')L^{\mu 5}\Big] \\
+ \langle\gamma(k)|\bar{s}i\sigma_{\mu\nu}q^\nu b|\bar{B}_s^0(p_B)\rangle \Big[-2m_b\frac{C_7^{\rm eff}}{q^2}L^\mu\Big] \\
+ \langle\gamma(k)|\bar{s}i\sigma_{\mu\nu}\gamma_5 q^\nu b|\bar{B}_s^0(p_B)\rangle \Big[-2m_b\frac{C_7^{\rm eff}}{q^2}L^\mu\Big] \\
+ \langle\gamma(k)|\bar{s}\sigma_{\mu\nu} b|\bar{B}_s^0(p_B)\rangle [2C_T L^{\mu\nu} + 2iC_{TE}\epsilon^{\mu\nu\alpha\beta}L_{\alpha\beta}] \Big\},
\end{aligned}
\tag{B.1}
$$

where the L's are defined in eq. (2.8).

In order to calculate the DBR, one needs the $\bar{B}_s^0 \to \gamma$ matrix elements and form factors. The matrix elements are given in ref. [40]:[3]

$$
\begin{aligned}
\langle\gamma(k)|\bar{s}\gamma_\mu b|\bar{B}_s^0(p_B)\rangle &= -e\,\epsilon_{\mu\nu\rho\sigma}\varepsilon^{*\nu}q^\rho k^\sigma\frac{f_V(q^2)}{m_{B_s}}, \\
\langle\gamma(k)|\bar{s}\gamma_\mu\gamma_5 b|\bar{B}_s^0(p_B)\rangle &= ie\big[\varepsilon_\mu^* k\cdot q - \varepsilon^*\cdot q k_\mu\big]\frac{f_A(q^2)}{m_{B_s}}, \\
\langle\gamma(k)|\bar{s}i\sigma_{\mu\nu}q^\nu b|\bar{B}_s^0(p_B)\rangle &= e\,\epsilon_{\mu\nu\rho\sigma}\varepsilon^{*\nu}q^\rho k^\sigma f_{TV}(q^2), \\
\langle\gamma(k)|\bar{s}i\sigma_{\mu\nu}\gamma_5 q^\nu b|\bar{B}_s^0(p_B)\rangle &= ie\big[\varepsilon_\mu^* k\cdot q - \varepsilon^*\cdot q k_\mu\big] f_{TA}(q^2), \\
\langle\gamma(k)|\bar{s}\sigma_{\mu\nu} b|\bar{B}_s^0(p_B)\rangle &= -ie\,\epsilon_{\mu\nu\rho\sigma}\Bigg[\frac{\{f_{TV}(q^2) - f_{TA}(q^2)\}}{q^2}\Big\{(q\cdot k)\,\varepsilon^{*\rho}\,q^\sigma + (\varepsilon^*\cdot q)\,q^\rho\,k^\sigma\Big\} \\
&\qquad - f_{TV}(q^2)\,\varepsilon^{*\rho}\,k^\sigma\Bigg].
\end{aligned}
\tag{B.2}
$$

Here ε_μ is the four-vector polarization of the photon and $q = p_B - k$. For the $\bar{B}_s^0 \to \mu^+\mu^-\gamma$ form factors f_i $(i = V, A, TA, TV)$, we use the parameterization [40]

$$
f_i(q^2) = \beta_i\frac{f_{B_s}m_{B_s}}{\Delta_i + 0.5m_{B_s}\left(1 - q^2/m_{B_s}^2\right)}, \tag{B.3}
$$

where the parameters β_i and Δ_i are given in table 2. These values of parameters ensure that the large energy effective theory (LEET) relations between form factors are satisfied to a 10% accuracy [40]. In our numerical analysis we take the errors in these form factors to be $\pm 10\%$.

[3] We use the convention $\epsilon^{0123} = +1$.

JHEP11(2011)121

Parameter	f_V	f_{TV}	f_A	f_{TA}
$\beta(\text{GeV}^{-1})$	0.28	0.30	0.26	0.33
$\Delta(\text{GeV})$	0.04	0.04	0.30	0.30

Table 2. The parameters for $\bar{B}_s^0 \to \gamma$ form factors, as defined in eq. (B.3).

In terms of the dimensionless parameter $x_\gamma = 2E_\gamma/m_{B_s}$, where E_γ is the photon energy in the $\bar{B}_s^0$ rest frame, one can calculate the double differential decay rate to be

$$\frac{\mathrm{d}^2\Gamma}{\mathrm{d}x_\gamma \mathrm{d}(\cos\theta_\mu)} = \frac{1}{2m_{B_s}} \frac{2v\, m_{B_s}^2 x_\gamma}{(8\pi)^3} \mathcal{M}^\dagger \mathcal{M} \,, \tag{B.4}$$

where $v \equiv \sqrt{1 - 4m_\mu^2/[m_{B_s}^2(1-x_\gamma)]}$. From eq. (B.4) we get the DBR to be

$$\begin{aligned} \frac{\mathrm{d}B}{\mathrm{d}x_\gamma} &= \tau_{B_s} \int_{-1}^{1} \frac{\mathrm{d}^2\Gamma}{\mathrm{d}x_\gamma \mathrm{d}(\cos\theta_\mu)} \,\mathrm{d}\cos\theta_\mu \\ &= \tau_{B_s} \left[\frac{1}{2m_{B_s}} \frac{2vm_{B_s}^2}{(8\pi)^3}\right] \left[\frac{1}{4}\, \frac{16G_F^2}{2} \frac{\alpha_{em}^2}{16\pi^2} |V_{tb}V_{ts}^*|^2 e^2\right] \Theta \,. \end{aligned} \tag{B.5}$$

Here the quantity Θ has the form

$$\Theta = \frac{2}{3}\, m_{B_s}^4\, x_\gamma^3 \Big[X_{VA} + X_T + X_{VA\text{-}T}\Big] \,, \tag{B.6}$$

where the X terms are

$$\begin{aligned} X_{VA} &= \Big(|A|^2 + |B|^2\Big) m_{B_s}^2 \left(3 - v^2\right)(1 - x_\gamma) + \Big(|C|^2 + |D|^2\Big) 2m_{B_s}^2 v^2 (1 - x_\gamma) \,, \\ X_T &= 4|E|^2(3 - v^2) + 4|F|^2 m_{B_s}^4 v^2 (1 - x_\gamma)^2 \\ &\quad + 16|G|^2 \left(3 - v^2\right) + 16|H|^2 m_{B_s}^4 \left(3 - 2v^2\right)(1 - x_\gamma)^2 \\ &\quad + 8m_{B_s}^2 v^2 (1 - x_\gamma) \mathrm{Re}\left(E^* F\right) + 32 m_{B_s}^2 (3 - 2v^2)(1 - x_\gamma) \mathrm{Re}\left(G^* H\right) \,, \\ X_{VA\text{-}T} &= -24 m_\mu \mathrm{Re}\left(A^* E\right) - 48 m_\mu \mathrm{Re}\left(B^* G\right) - 48 m_\mu m_{B_s}^2 (1 - x_\gamma) \mathrm{Re}\left(B^* H\right) \,. \end{aligned} \tag{B.7}$$

Note that here, the VA subscript includes the SM operators. The parameters A–H are combinations of the Wilson coefficients, form factors and NP parameters, and are given by

$$\begin{aligned} A &= (C_9^{\text{eff}} + R_V + R_V') \frac{f_V(q^2)}{m_{B_s}} + \frac{2\, m_b C_7^{\text{eff}}}{q^2} f_{TV}(q^2) \,, \\ B &= (C_9^{\text{eff}} + R_V - R_V') \frac{f_A(q^2)}{m_{B_s}} + \frac{2\, m_b C_7^{\text{eff}}}{q^2} f_{TA}(q^2) \,, \\ C &= (C_{10}^{\text{eff}} + R_A + R_A') \frac{f_V(q^2)}{m_{B_s}} \,, \\ D &= (C_{10}^{\text{eff}} + R_A - R_A') \frac{f_A(q^2)}{m_{B_s}} \,, \end{aligned}$$

JHEP11(2011)121

$$
\begin{aligned}
E &= -2C_T f_{TV}(q^2)\,, \\
F &= 2C_T \frac{f_{TV}(q^2) - f_{TA}(q^2)}{q^2}\,, \\
G &= -2C_{TE} f_{TV}(q^2)\,, \\
H &= 2C_{TE} \frac{f_{TV}(q^2) - f_{TA}(q^2)}{q^2}\quad .
\end{aligned}
\tag{B.8}
$$

The normalized forward-backward asymmetry of muons in $\bar{B}_s^0 \to \mu^+\mu^-\gamma$ is defined as

$$
A_{FB}(q^2) = \frac{\displaystyle\int_0^1 d\cos\theta_\mu \frac{d^2B}{dq^2 d\cos\theta_\mu} - \int_{-1}^0 d\cos\theta_\mu \frac{d^2B}{dq^2 d\cos\theta_\mu}}{\displaystyle\int_0^1 d\cos\theta_\mu \frac{d^2B}{dq^2 d\cos\theta_\mu} + \int_{-1}^0 d\cos\theta_\mu \frac{d^2B}{dq^2 d\cos\theta_\mu}}\,,
\tag{B.9}
$$

where θ_μ is the angle between the three-momentum vectors of the $\bar{B}_s^0$ and the μ^+ in the dimuon center-of-mass frame. The calculation of A_{FB} gives

$$
A_{FB}(q^2) = \frac{1}{\Theta}\left(2m_{B_s}^4 v\, x_\gamma^3\right)\Big[Y_{VA} + Y_{VA\text{-}T}\Big]\,,
\tag{B.10}
$$

with the Y terms given by

$$
\begin{aligned}
Y_{VA} &= \Big(\mathrm{Re}\,(A^*D) + \mathrm{Re}\,(B^*C)\Big) m_{B_s}^2 (1-x_\gamma)\,, \\
Y_{VA\text{-}T} &= -4m_\mu\Big(2\mathrm{Re}\,(C^*G) + 2m_{B_s}^2(1-x_\gamma)\mathrm{Re}\,(C^*H) + \mathrm{Re}\,(D^*E)\Big)\,.
\end{aligned}
\tag{B.11}
$$

C Details of the $\bar{B}_d^0 \to \bar{K}\mu^+\mu^-$ analysis

The transition matrix element for $\bar{B}_d^0 \to \bar{K}\mu^+\mu^-$ is given by

$$
\begin{aligned}
i\mathcal{M}\,(\bar{B}_d^0 \to \bar{K}\mu^+\mu^-) = (-i)\,\frac{1}{2}\,\Bigg[-\frac{4\,G_F}{\sqrt{2}}\frac{\alpha_{em}}{4\pi}(V_{ts}^* V_{tb})\Bigg] \times \\
\Big\{\langle K(p_2)\,|\bar{s}\gamma_\mu b|\,B(p_1)\rangle\,[(C_9^{\mathrm{eff}} + R_V + R_V')L^\mu + (C_{10} + R_A + R_A')L^{\mu 5}] \\
+ \langle K(p_2)\,|\bar{s}b|\,B(p_1)\rangle\,[(R_S + R_S')L + (R_P + R_P')L^5] \\
+ \langle K(p_2)\,|\bar{s}i\sigma_{\mu\nu}q^\nu b|\,B(p_1)\rangle\,[-2C_7^{\mathrm{eff}}(m_b/q^2)L^\mu] \\
+ \langle K(p_2)\,|\bar{s}\sigma_{\mu\nu}b|\,B(p_1)\rangle\;\,[2C_T L^{\mu\nu} + 2iC_{TE}\epsilon^{\mu\nu\alpha\beta}L_{\alpha\beta}]\Big\}\,,
\end{aligned}
\tag{C.1}
$$

where the L's are defined in eq. (2.8).

JHEP11(2011)121

The $\bar{B}^0_d \to \bar{K}$ matrix elements needed to calculate the decay rate and asymmetry in $\bar{B}^0_d \to \bar{K}\mu^+\mu^-$ are [45]

$$\begin{aligned}
\left\langle \bar{K}(p_2)\,|\bar{s}\gamma_\mu b|\,\bar{B}^0_d(p_1)\right\rangle &= (2p_1-q)_\mu f_+(z) + \left(\frac{1-k^2}{z}\right) q_\mu [f_0(z) - f_+(z)]\,, \\
\left\langle \bar{K}(p_2)\,|\bar{s}i\sigma_{\mu\nu}q^\nu b|\,\bar{B}^0_d(p_1)\right\rangle &= -\Big[(2p_1-q)_\mu q^2 - (m_B^2 - m_K^2)q_\mu\Big]\,\frac{f_T(z)}{m_B+m_K}\,, \\
\left\langle \bar{K}(p_2)\,|\bar{s}b|\,\bar{B}^0_d(p_1)\right\rangle &= \frac{m_B(1-k^2)}{\hat{m}_b} f_0(z)\,, \\
\left\langle \bar{K}(p_2)\,|\bar{s}\sigma_{\mu\nu}b|\,\bar{B}^0_d(p_1)\right\rangle &= i\Big[(2p_1-q)_\mu q_\nu - (2p_1-q)_\nu q_\mu\Big]\,\frac{f_T(z)}{m_B+m_K}\,,
\end{aligned} \tag{C.2}$$

where $k \equiv m_K/m_B$, $\hat{m}_b \equiv m_b/m_B$, $q_\mu = (p_1-p_2)_\mu = (p_+ + p_-)_\mu$, and $z \equiv q^2/m_B^2$. The form factors $f_{+,0,T}$ were calculated in the framework of QCD light-cone sum rules in ref. [45]. The z dependence of these is parametrized by

$$f(z) = f(0)\,\exp(c_1 z + c_2 z^2 + c_3 z^3)\,, \tag{C.3}$$

where the parameters $f(0), c_1$, c_2 and c_3 for each form factor are taken from tables III, IV and V of ref. [45]. Using these, the differential branching ratio is given by

$$\frac{dB}{dz} = B'_0\,\phi^{1/2}\,\beta_\mu \Big[X'_{VA} + X'_{SP} + X'_T + X'_{VA\text{-}SP} + X'_{VA\text{-}T}\Big]\,, \tag{C.4}$$

where B'_0 is the normalization factor:

$$B'_0 = \frac{G_F^2\alpha^2\tau_B}{2^{12}\pi^5}|V_{tb}V_{ts}^*|^2 m_B^5\,, \tag{C.5}$$

the phase factor ϕ is

$$\phi \equiv 1 + k^4 + z^2 - 2(k^2 + k^2 z + z)\,, \tag{C.6}$$

and the X' terms are given by

$$\begin{aligned}
X'_{VA} &= \phi\left(1 - \frac{1}{3}\beta_\mu^2\right)(|A'|^2 + |B'|^2) \;+\; 4\,\hat{m}_\mu^2\,|B'|^2\,(2 + 2k^2 - z) \\
&\quad + 4\,\hat{m}_\mu^2\,z\,|C'|^2 \;+\; 8\,\hat{m}_\mu^2\,(1-k^2)\,\mathrm{Re}(B'C'^*)\,, \\
X'_{SP} &= \frac{z}{m_B^2}\,(|E'|^2 + \beta_\mu^2\,|D'|^2)\,, \\
X'_T &= \frac{4}{3}\,\phi\,z\,m_B^2\,\Big[3|F'|^2 \;+\; 2\,\beta_\mu^2\,(2|G'|^2 - |F'|^2)\Big]\,, \\
X'_{VA\text{-}SP} &= \frac{4\hat{m}_\mu}{m_B}\,(1-k^2)\,\mathrm{Re}(B'E'^*) + \frac{4\hat{m}_\mu}{m_B}\,z\,\mathrm{Re}(C'E'^*)\,, \\
X'_{VA\text{-}T} &= 8\hat{m}_\mu\,m_B\phi\,\mathrm{Re}(A'F'^*)\,.
\end{aligned} \tag{C.7}$$

Here $\hat{m}_\mu \equiv m_\mu/m_B$ and $\beta_\mu \equiv \sqrt{1 - 4\hat{m}_\mu^2/z}$. The parameters A'–G' are combinations of

JHEP11(2011)121

the Wilson coefficients, form factors and NP parameters, and are given by

$$\begin{aligned}
A' &\equiv 2(C_9^{\rm eff} + R_V + R'_V)\, f_+(z) + 4C_7^{\rm eff}\hat{m}_b \frac{f_T(z)}{1+k}\,, \\
B' &\equiv 2(C_{10} + R_A + R'_A)\, f_+(z)\,, \\
C' &\equiv 2(C_{10} + R_A + R'_A)\, \frac{1-k^2}{z}\big[f_0(z) - f_+(z)\big]\,, \\
D' &\equiv 2(R_S + R'_S)\frac{m_B(1-k^2)}{\hat{m}_b} f_0(z)\,, \\
E' &\equiv 2(R_P + R'_P)\frac{m_B(1-k^2)}{\hat{m}_b} f_0(z)\,, \\
F' &\equiv 4C_T \frac{f_T(z)}{m_B(1+k)}\,, \\
G' &\equiv -4C_{TE}\frac{f_T(z)}{m_B(1+k)}\,.
\end{aligned} \tag{C.8}$$

The limits on the kinematical variables z and $\cos\theta_\mu$ are

$$-1 \le \cos\theta_\mu \le 1\ , \qquad 4\hat{m}_\mu^2 \le z \le (1-k)^2\,. \tag{C.9}$$

Note that in the large energy (LEET) limit, there are relations between form factors that are valid up to α_s, $1/E_K$ and $1/m_b$ corrections [50, 51]. These are

$$\begin{aligned}
f_+(z) &= \zeta(m_B, E_P), \\
f_0(z) &= \left(1 - \frac{q^2}{m_B^2 - m_P^2}\right)\zeta(m_B, E_P), \\
f_T(z) &= \left(1 + \frac{m_P}{m_B}\right)\zeta(m_B, E_P)\,.
\end{aligned} \tag{C.10}$$

Thus, all form factors can be expressed in terms of a single universal soft form factor $\zeta(m_B, E_P)$ in this limit.

The normalized forward-backward asymmetry for the muons in $\bar{B}_d^0 \to \bar{K}\mu^+\mu^-$ is defined as

$$A_{FB}(q^2) = \frac{\displaystyle\int_0^1 d\cos\theta_\mu \frac{d^2B}{dq^2 d\cos\theta_\mu} - \int_{-1}^0 d\cos\theta_\mu \frac{d^2B}{dq^2 d\cos\theta_\mu}}{\displaystyle\int_0^1 d\cos\theta_\mu \frac{d^2B}{dq^2 d\cos\theta_\mu} + \int_{-1}^0 d\cos\theta_\mu \frac{d^2B}{dq^2 d\cos\theta_\mu}}\,, \tag{C.11}$$

where θ_μ is the angle between the three-momenta of the $\bar{B}_d^0$ and the μ^+ in the dimuon center-of-mass frame. The calculation of $A_{FB}(q^2)$ gives

$$A_{FB}(q^2) = \frac{2B'_0\,\beta_\mu\,\phi}{dB/dz}\Big[Y'_{VA\text{-}SP} + Y'_{VA\text{-}T} + Y'_{SP\text{-}T}\Big] \tag{C.12}$$

where

$$\begin{aligned}
Y'_{VA\text{-}SP} &= -\frac{\hat{m}_\mu}{m_B}{\rm Re}(A'D'^*) \\
Y'_{VA\text{-}T} &= -4m_\mu(1-k^2){\rm Re}(B'G'^*) - 4zm_\mu{\rm Re}(C'G'^*) \\
Y'_{SP\text{-}T} &= -\frac{z}{4}{\rm Re}(D'F'^*) - 2z{\rm Re}(E'G'^*)\,.
\end{aligned} \tag{C.13}$$

Note that only $Y'_{SP\text{-}T}$ term is unsuppressed by the muon mass.

JHEP11(2011)121

D Details of the $\bar{B}^0_d \to \bar{K}^* \mu^+ \mu^-$ angular analysis

D.1 Matrix elements

The full transition amplitude for $\bar{B}(p_B) \to \bar{K}^*(p_{K^*}, \epsilon^*)\mu^+(p_\mu^+)\mu^-(p_\mu^-)$ is

$$
\begin{aligned}
i\mathcal{M}\,(\bar{B}^0_d \to \bar{K}^*\mu^+\mu^-) = (-i)\,\frac{1}{2}\Bigg[-\frac{4\,G_F}{\sqrt{2}}\frac{\alpha_{em}}{4\pi}(V_{ts}^*V_{tb})\Bigg] \times \\
\Big\{\langle K^*(p_{K^*},\epsilon)|\bar{s}\gamma_\mu b|B(p_B)\rangle\,[(C_9^{\rm eff}+R_V+R'_V)L^\mu + (C_{10}+R_A+R'_A)L^{\mu 5}] \\
+\langle K^*(p_{K^*},\epsilon)|\bar{s}\gamma_\mu\gamma_5 b|B(p_B)\rangle[-(C_9^{\rm eff}+R_V-R'_V)L^\mu - (C_{10}+R_A-R'_A)L^{\mu 5}] \\
+\langle K^*(p_{K^*},\epsilon)|\bar{s}i\sigma_{\mu\nu}q^\nu(1+\gamma_5)b|B(p_B)\rangle\,[-2C_7^{\rm eff}(m_b/q^2)L^\mu] \\
+\langle K^*(p_{K^*},\epsilon)|\bar{s}b|B(p_B)\rangle\,[(R_S+R'_S)L + (R_P+R'_P)L^5] \\
+\langle K^*(p_{K^*},\epsilon)|\bar{s}\gamma_5 b|B(p_B)\rangle\,[(R_S-R'_S)L + (R_P-R'_P)L^5] \\
+\langle K^*(p_{K^*},\epsilon)|\bar{s}\sigma_{\mu\nu}b|B(p_B)\rangle\,[2C_T L^{\mu\nu} + 2iC_{TE}\epsilon^{\mu\nu\alpha\beta}L_{\alpha\beta}]\Big\}\,,
\end{aligned}
\tag{D.1}
$$

where the L's are defined in eq. (2.8). Here $q = p_B - p_{K^*} = p_\mu^+ + p_\mu^-$. This can be written in the form

$$
\begin{aligned}
i\mathcal{M}(\bar{B}^0_d \to \bar{K}^*\mu^+\mu^-) = (-i)\frac{1}{2}\Bigg[\frac{4\,G_F}{\sqrt{2}}\frac{\alpha_{em}}{4\pi}(V_{ts}^*V_{tb})\Bigg] \times \\
[M_{V\mu}L^\mu + M_{A\mu}L^{\mu 5} + M_S L + M_P L^5 + M_{T\mu\nu}L^{\mu\nu} + iM_{E\mu\nu}L_{\alpha\beta}\epsilon^{\mu\nu\alpha\beta}]\,,
\end{aligned}
\tag{D.2}
$$

with

$$
\begin{aligned}
M_{V\mu} &= -A''\epsilon_{\mu\nu\alpha\beta}\varepsilon^{*\nu}p_{K^*}^\alpha q^\beta + iB''\varepsilon_\mu^* + iC''\varepsilon^*.q(p_B+p_{K^*})_\mu + iD''\varepsilon^*.q q_\mu, \\
M_{A\mu} &= -E''\epsilon_{\mu\nu\alpha\beta}\varepsilon^{*\nu}p_{K^*}^\alpha q^\beta + iF''\varepsilon_\mu^* + iG''\varepsilon^*.q(p_B+p_{K^*})_\mu + iH''\varepsilon^*.q q_\mu, \\
M_S &= iS''\varepsilon^*.q, \\
M_P &= iP''\varepsilon^*.q, \\
M_{T\mu\nu} &= C_T(iT_1''\epsilon_{\mu\nu\alpha\beta}\varepsilon^{*\alpha}(p_B+p_{K^*})^\beta + iT_2''\epsilon_{\mu\nu\alpha\beta}\varepsilon^{*\alpha}q^\beta - iT_3''\epsilon_{\mu\nu\alpha\beta}\varepsilon^*.q p_{K^*}^\alpha q^\beta), \\
M_{E\mu\nu} &= C_{TE}(iT_1''\epsilon_{\mu\nu\alpha\beta}\varepsilon^{*\alpha}(p_B+p_{K^*})^\beta + iT_2''\epsilon_{\mu\nu\alpha\beta}\varepsilon^{*\alpha}q^\beta - iT_3''\epsilon_{\mu\nu\alpha\beta}\varepsilon^*.q p_{K^*}^\alpha q^\beta)\,.
\end{aligned}
\tag{D.3}
$$

The quantities A'', B'', C'', D'',E'', F'', G'', S'', P'', and T_i'' (1=1,2,3) are related to the $\bar{B} \to \bar{K}^*$ form factors which are given below. The contribution to the transition amplitudes from the quantity $D''(q^2)$ vanishes and that from $H''(q^2)$ is suppressed because of the equation of motion of the muons.

D.2 Form factors

The form factors for the decay amplitude for $\bar{B}^0_d \to \bar{K}^*\mu^+\mu^-$ [eq. (D.1)] in terms of matrix elements of the quark operators are given by [45]

$$
\begin{aligned}
\langle K^*(p_{K^*},\epsilon)|\bar{s}\gamma_\mu(1\pm\gamma_5)b|B(p_B)\rangle &= \mp\, iq_\mu\frac{2m_{K^*}}{q^2}\,\epsilon^*\cdot q\,\Big[A_3(q^2)-A_0(q^2)\Big] \\
&\pm i\epsilon_\mu^*(m_B+m_{K^*})A_1(q^2) \mp\; i(p_B+p_{K^*})_\mu\,\epsilon^*\cdot q\,\frac{A_2(q^2)}{(m_B+m_{K^*})} \\
&- \epsilon_{\mu\nu\lambda\sigma}\epsilon^{*\nu}p_{K^*}^\lambda q^\sigma\frac{2V(q^2)}{(m_B+m_{K^*})}\,,
\end{aligned}
\tag{D.4}
$$

JHEP11(2011)121

where

$$A_3(q^2) = \frac{m_B + m_{K^*}}{2m_{K^*}} A_1(q^2) - \frac{m_B - m_{K^*}}{2m_{K^*}} A_2(q^2)\,. \tag{D.5}$$

$$\begin{aligned}\langle K^*(p_{K^*},\epsilon)|\bar{s}\sigma_{\mu\nu}b|B(p_B)\rangle \;=\; & i\epsilon_{\mu\nu\lambda\sigma}\Big\{ -T_1(q^2)\epsilon^{*\lambda}(p_B+p_{K^*})^\sigma \\ & + \frac{(m_B^2-m_{K^*}^2)}{q^2}\big(T_1(q^2)-T_2(q^2)\big)\epsilon^{*\lambda}q^\sigma \\ & - \frac{2}{q^2}\left(T_1(q^2) - T_2(q^2) - \frac{q^2}{(m_B^2-m_{K^*}^2)}T_3(q^2)\right)\epsilon^*\cdot q\, p_{K^*}^\lambda q^\sigma\Big\}\,.\end{aligned} \tag{D.6}$$

$$\begin{aligned}\langle K^*(p_{K^*},\epsilon)|\bar{s}i\sigma_{\mu\nu}q^\nu(1\pm\gamma_5)b|B(p_B)\rangle \;=\; & 2\epsilon_{\mu\nu\lambda\sigma}\epsilon^{*\nu}p_{K^*}^\lambda q^\sigma\; T_1(q^2) \\ & \pm i\Big\{\epsilon_{*\mu}(m_B^2-m_{K^*}^2) - (p_B+p_{K^*})_\mu \epsilon^*\cdot q\Big\}\; T_2(q^2) \\ & \pm i\,\epsilon^*\cdot q\left\{q_\mu - \frac{(p_B+p_{K^*})_\mu q^2}{(m_B^2-m_{K^*}^2)}\right\} T_3(q^2)\,.\end{aligned} \tag{D.7}$$

$$\langle K^*(p_{K^*},\epsilon)|\bar{s}(1\pm\gamma_5)b|B(p_B)\rangle \;=\; \mp\, 2i\frac{m_{K^*}}{m_b}\,\epsilon^*\cdot q\, A_0(q^2)\,. \tag{D.8}$$

Here we have neglected the strange-quark mass. The matrix elements are functions of 7 unknown form factors: $A_{0,1,2}(q^2)$, $V(q^2)$, $T_{1,2,3}(q^2)$.

The matrix elements $M_{V,A,S,P,T,E}$ appearing in eq. (D.3) can be written in terms of these 7 form factors, coupling constants and kinematic variables as

$$\begin{aligned}
A'' &= \left[\frac{2V(q^2)(C_9^{\rm eff}+R_V+R_V')}{m_B+m_{K^*}} + \frac{4m_b}{q^2}C_7^{\rm eff}T_1(q^2)\right],\\
B'' &= -\left[(m_B+m_{K^*})A_1(q^2)(C_9^{\rm eff}+R_V-R_V') + \frac{2m_b}{q^2}C_7^{\rm eff}T_2(q^2)(m_B^2-m_{K^*}^2)\right],\\
C'' &= \left[\frac{A_2(q^2)}{m_B+m_{K^*}}(C_9^{\rm eff}+R_V-R_V') + \frac{2m_b}{q^2}C_7^{\rm eff}\left(T_2(q^2)+\frac{q^2T_3(q^2)}{(m_B^2-m_{K^*}^2)}\right)\right],\\
D'' &= \left[\frac{2m_{K^*}}{q^2}(C_9^{\rm eff}+R_V-R_V')(A_3(q^2)-A_0(q^2)) - \frac{2m_b}{q^2}C_7^{\rm eff}T_3(q^2)\right],\\
E'' &= \left[\frac{2V(q^2)(C_{10}+R_A+R_A')}{m_B+m_{K^*}}\right],\\
F'' &= -\Big[(m_B+m_{K^*})A_1(q^2)(C_{10}+R_A-R_A')\Big],\\
G'' &= \left[\frac{A_2(q^2)}{m_B+m_{K^*}}(C_{10}+R_A-R_A')\right],\\
H'' &= \left[\frac{2m_{K^*}}{q^2}(C_{10}+R_A-R_A')(A_3(q^2)-A_0(q^2))\right],\\
S'' &= \left[-2(R_S-R_S')\frac{m_{K^*}}{m_b}A_0(q^2)\right],\\
P'' &= \left[-2(R_P-R_P')\frac{m_{K^*}}{m_b}A_0(q^2)\right],\\
T_1'' &= -2T_1(q^2),
\end{aligned}$$

JHEP11(2011)121

$$T_2'' = \left[\frac{2(m_B^2 - m_{K^*}^2)}{q^2}(T_1(q^2) - T_2(q^2))\right],$$
$$T_3'' = \left[\frac{4}{q^2}\left(T_1(q^2) - T_2(q^2) - \frac{q^2 T_3(q^2)}{m_B^2 - m_{K^*}^2}\right)\right]. \tag{D.9}$$

Also, we define

$$T_0 = \frac{1}{m_{K^*}}\left(\sqrt{q^2}(E_{K^*}\sqrt{q^2} + 2m_{K^*}^2)T_1'' + q^2(E_{K^*}T_2'' - |\vec{p}_{K^*}|^2\sqrt{q^2}T_3'')\right),$$
$$T_+ = (q^2 + 2E_{K^*}\sqrt{q^2})T_1'' + q^2 T_2'', \quad T_- = 2|\vec{p}_{K^*}|\sqrt{q^2}T_1'' . \tag{D.10}$$

D.3 Transversity amplitudes

We summarize the various transversity amplitudes that appear in the $\bar{B}_d^0 \to \bar{K}^*\mu^+\mu^-$ angular distribution. The decay amplitude of $\bar{B}_d^0 \to \bar{K}^*\mu^+\mu^-$ depends on the K^* polarization vector $\varepsilon(\lambda)$ with helicity λ $(0, \pm 1)$. Hence, the decay amplitude can be decomposed into three components. Below we define the helicity amplitudes of various operators with different Lorentz structures (V, A, S, P, T, TE) in eq. (D.1).

$$A_V^0 = \sqrt{q^2}\left(\frac{E_{K^*}}{m_{K^*}}B'' + \frac{2|\vec{p}_{K^*}|^2\sqrt{q^2}}{m_{K^*}}C''\right), \qquad A_V^\pm = \sqrt{q^2}(\pm|\vec{p}_{K^*}|\sqrt{q^2}A'' + B''),$$
$$A_A^0 = \sqrt{q^2}\left(\frac{E_{K^*}}{m_{K^*}}F'' + \frac{2|\vec{p}_{K^*}|^2\sqrt{q^2}}{m_{K^*}}G''\right), \qquad A_A^\pm = \sqrt{q^2}(\pm|\vec{p}_{K^*}|\sqrt{q^2}E'' + F''),$$
$$A_S = \frac{2|\vec{p}_{K^*}|q^2}{m_{K^*}}S'', \qquad A_P = \frac{2|\vec{p}_{K^*}|q^2}{m_{K^*}}P'',$$
$$A_T^0 = T_0 C_T, \qquad A_T^\pm = T_\pm C_T,$$
$$A_{TE}^0 = 2T_0 C_{TE}, \qquad A_{TE}^\pm = 2T_\pm C_{TE},$$
$$A_{vt} = -2|\vec{p}_{K^*}|\sqrt{q^2}(C_{10} + R_A - R_{A'})A_0, \tag{D.11}$$

where the amplitude A_{vt} is related to the time-like component of the virtual K^*. In the transversity basis, the positive and negative helicity amplitudes are replaced by the transversity amplitudes as

$$A_\parallel^i = \frac{1}{2}(A_i^+ + A_i^-), \quad A_\perp^i = \frac{1}{2}(A_i^+ - A_i^-), \qquad \mathrm{i} = \mathrm{V, A, T, TE}. \tag{D.12}$$

The left and right component of the transversity amplitudes of vector and axial-vector currents in [61] can be written as

$$A_{0,VA}^{L,R} = A_V^0 \mp A_A^0, A_{\parallel,VA}^{L,R} = (A_\parallel^V \mp A_\parallel^A), A_{\perp,VA}^{L,R} = (A_\perp^V \mp A_\perp^A) . \tag{D.13}$$

Note that in the notation of ref. [61], we have the correspondence $A_{(0,\parallel,\perp),VA}^{L,R} = (\sqrt{q^2}/N)A_{(0,\parallel,\perp)}^{L,R}$. The amplitudes $A_{S,P,vt}$ remain the same, while $A_S = -(\sqrt{q^2}/N)A_S^{L,R}$.

JHEP11(2011)121

D.4 Angular coefficients

The expressions for the twelve angular coefficients (I's) in the $\bar{B}^0_d \to \bar{K}^*\mu^+\mu^-$ angular distribution are summarized here according to K^* helicity combinations $\lambda_1\lambda_2$. The longitudinal I^0's ($\lambda_1\lambda_2 = 00$) are given by

$$
\begin{aligned}
I^0_1 &= 2\Bigg[\frac{1}{2}(|A^L_{0,VA}|^2 + |A^R_{0,VA}|^2) + \frac{1}{2}(\beta_\mu^2|A_S|^2 + |A_P|^2) + 4\beta_\mu^2(|A^0_T|^2 + |A^0_{TE}|^2) \\
&\quad + \frac{4m_\mu^2}{q^2}\Big(\mathrm{Re}[A^L_{0,VA}A^{R*}_{0,VA}] + 2|A_{vt}|^2 + 8|A^0_{TE}|^2\Big) \\
&\quad + \frac{4m_\mu}{\sqrt{q^2}}\Big(2\mathrm{Re}[(A^L_{0,VA} + A^R_{0,VA})A^{0*}_{TE}] - \mathrm{Re}[A_{vt}A_P^*]\Big)\Bigg], \qquad \text{(D.14)} \\
I^0_2 &= \beta_\mu^2\Big[-(|A^L_{0,VA}|^2 + |A^R_{0,VA}|^2) + 8(|A^0_T|^2 + |A^0_{TE}|^2)\Big], \\
I^0_3 &= 2\beta_\mu\Bigg[4(-\mathrm{Re}[A^0_{TE}A_S^*] + \mathrm{Re}[A^0_T A_P^*]) - \frac{4m_\mu}{\sqrt{q^2}}\Big(\frac{1}{2}\mathrm{Re}[(A^L_{0,VA} + A^R_{0,VA})A_S^*] + 4\mathrm{Re}[A_{vt}A^{0*}_T]\Big)\Bigg].
\end{aligned}
$$

The transverse I^T's ($\lambda_1\lambda_2 = ++, --, +-, -+$) are given by

$$
\begin{aligned}
I^T_1 &= \Bigg[\frac{2+\beta_\mu^2}{2}\Big(|A^V_\parallel|^2 + |A^V_\perp|^2 + |A^A_\parallel|^2 + |A^A_\perp|^2\Big) - 4(-2+\beta_\mu^2)\Big(|A^T_\parallel|^2 + |A^T_\perp|^2 + |A^{TE}_\parallel|^2 \\
&\quad + |A^{TE}_\perp|^2\Big) + \frac{4m_\mu^2}{q^2}\Big(|A^V_\parallel|^2 + |A^V_\perp|^2 - |A^A_\parallel|^2 - |A^A_\perp|^2 - 16(A^T_\parallel A^{T*}_\perp - A^{TE}_\parallel A^{TE*}_\perp)\Big) \\
&\quad + 16\frac{m_\mu}{\sqrt{q^2}}\Big(\mathrm{Re}[A^V_\perp(A^{T*}_\parallel - A^{T*}_\perp)] + \mathrm{Re}[A^V_\parallel(A^{TE*}_\parallel + A^{TE*}_\perp)]\Big)\Bigg], \\
I^T_2 &= \beta_\mu^2\Bigg[\frac{1}{2}\Big(|A^V_\parallel|^2 + |A^V_\perp|^2 + |A^A_\parallel|^2 + |A^A_\perp|^2\Big) - 4\Big(|A^T_\parallel|^2 + |A^T_\perp|^2 + |A^{TE}_\parallel|^2 + |A^{TE}_\perp|^2\Big)\Bigg], \\
I^T_3 &= -4\beta_\mu\Bigg[\mathrm{Re}[A^V_\perp A^{A*}_\parallel + A^V_\parallel A^{A*}_\perp] + 4\frac{m_\mu}{\sqrt{q^2}}\mathrm{Re}[A^A_\parallel(A^{T*}_\parallel - A^{T*}_\perp) + A^A_\perp(A^{TE*}_\parallel + A^{TE*}_\perp)]\Bigg], \\
I^T_4 &= \beta_\mu^2\Big[\Big(|A^V_\perp|^2 - |A^V_\parallel|^2 + |A^A_\perp|^2 - |A^A_\parallel|^2\Big) + 16\Big(A^T_\parallel A^{T*}_\perp + A^{TE}_\parallel A^{TE*}_\perp\Big)\Big], \\
I^T_5 &= 2\beta_\mu^2\mathrm{Im}[A^{V*}_\parallel A^V_\perp + A^{A*}_\parallel A^A_\perp]\,. \qquad \text{(D.15)}
\end{aligned}
$$

The mixed I^{LT}'s ($\lambda_1\lambda_2 = 0\pm, \pm 0$) are given by

$$
\begin{aligned}
I^{LT}_1 &= \beta_\mu^2\Bigg[\frac{1}{\sqrt{2}}\mathrm{Re}[A^R_{0,VA}(A^{V*}_\parallel + A^{A*}_\parallel) + A^L_{0,VA}(A^{V*}_\parallel - A^{A*}_\parallel)] \\
&\quad - 4\sqrt{2}\Big(A^0_T(A^{T*}_\parallel + A^{T*}_\perp) + A^0_{TE}(A^{TE*}_\parallel + A^{TE*}_\perp)\Big)\Bigg], \\
I^{LT}_2 &= \frac{1}{\sqrt{2}}\beta_\mu^2\mathrm{Im}[A^R_{0,VA}(A^{V*}_\perp + A^{A*}_\perp) + A^L_{0,VA}(A^{V*}_\perp - A^{A*}_\perp)], \\
I^{LT}_3 &= \sqrt{2}\beta_\mu\Bigg[\mathrm{Re}[A^L_{0,VA}(A^{V*}_\perp - A^{A*}_\perp) - A^R_{0,VA}(A^{V*}_\perp + A^{A*}_\perp)] + 2\mathrm{Re}[(A^{TE}_\parallel + A^{TE}_\perp)A_S^*] \\
&\quad - 2\mathrm{Re}[(A^T_\parallel + A^T_\perp)A_P^*] + 2\frac{m_\mu}{\sqrt{q^2}}\mathrm{Re}[A^V_\parallel A_S^*]\Bigg],
\end{aligned}
$$

JHEP11(2011)121

$$I_4^{LT} = \sqrt{2}\beta_\mu \Big[\mathrm{Im}[A^L_{0,VA}(A^{V*}_\parallel - A^{A*}_\parallel) - A^R_{0,VA}(A^{V*}_\parallel + A^{A*}_\parallel)] + 2\mathrm{Im}[(A^T_\parallel - A^T_\perp)A^*_S] + 2\mathrm{Im}[(A^{TE}_\parallel - A^{TE}_\perp)A^*_P] - 2\frac{m_\mu}{\sqrt{q^2}}\mathrm{Im}[A^V_\perp A^*_S] \Big] . \quad \text{(D.16)}$$

References

[1] In the latest update of the πK puzzle, it was seen that, although NP was hinted at in $B \to \pi K$ decays, it could be argued that the SM can explain the data, see S. Baek, C.-W. Chiang and D. London, *The $B \to \pi K$ Puzzle: 2009 Update*, *Phys. Lett.* **B 675** (2009) 59 [arXiv:0903.3086] [INSPIRE].

[2] H.-Y. Cheng, C.-K. Chua and A. Soni, *CP-violating asymmetries in B^0 decays to $K^+K^-K^0_{S,L}$ and $K^0_SK^0_SK^0_{S,L}$*, *Phys. Rev.* **D 72** (2005) 094003 [hep-ph/0506268] [INSPIRE].

[3] G. Buchalla, G. Hiller, Y. Nir and G. Raz, *The Pattern of CP asymmetries in $b \to s$ transitions*, *JHEP* **09** (2005) 074 [hep-ph/0503151] [INSPIRE].

[4] E. Lunghi and A. Soni, *Hints for the scale of new CP-violating physics from B-CP anomalies*, *JHEP* **08** (2009) 051 [arXiv:0903.5059] [INSPIRE].

[5] CDF collaboration, T. Aaltonen et al., D0 collaboration, V.M. Abazov et al., *Combination of D0 and CDF Results on $\Delta\Gamma_s$ and the CP-Violating Phase $\beta_s^{J/\psi\phi}$*, CDF Note No. CDF/PHYS/BOTTOM/CDFR/9787 (2009), D0 Note No. 5928-CONF (2009).

[6] BABAR collaboration, B. Aubert et al., *Rates, polarizations and asymmetries in charmless vector-vector B meson decays*, *Phys. Rev. Lett.* **91** (2003) 171802 [hep-ex/0307026] [INSPIRE].

[7] BELLE collaboration, K. Chen et al., *Measurement of branching fractions and polarization in $B \to \phi K^{(*)}$ decays*, *Phys. Rev. Lett.* **91** (2003) 201801 [hep-ex/0307014] [INSPIRE].

[8] D0 collaboration, V.M. Abazov et al., *Evidence for an anomalous like-sign dimuon charge asymmetry*, *Phys. Rev.* **D 82** (2010) 032001 [arXiv:1005.2757] [INSPIRE].

[9] A. Dighe, A. Kundu and S. Nandi, *Enhanced $B_s - \bar{B}_s$ lifetime difference and anomalous like-sign dimuon charge asymmetry from new physics in $B_s \to \tau^+\tau^-$*, *Phys. Rev.* **D 82** (2010) 031502 [arXiv:1005.4051] [INSPIRE].

[10] BELLE collaboration, A. Ishikawa et al., *Measurement of Forward-Backward Asymmetry and Wilson Coefficients in $B \to K^*\ell^+\ell^-$*, *Phys. Rev. Lett.* **96** (2006) 251801 [hep-ex/0603018] [INSPIRE].

[11] BELLE collaboration, J.-T. Wei et al., *Measurement of the Differential Branching Fraction and Forward-Backword Asymmetry for $B \to K^{(*)}\ell^+\ell^-$*, *Phys. Rev. Lett.* **103** (2009) 171801 [arXiv:0904.0770] [INSPIRE].

[12] CDF collaboration, T. Aaltonen et al., *Measurement of the Forward-Backward Asymmetry in the $B \to K^{(*)}\mu^+\mu^-$ Decay and First Observation of the $B^0_s \to \phi\mu^+\mu^-$ Decay*, *Phys. Rev. Lett.* **106** (2011) 161801 [arXiv:1101.1028] [INSPIRE].

[13] BABAR collaboration, B. Aubert et al., *Measurements of branching fractions, rate asymmetries and angular distributions in the rare decays $B \to K\ell^+\ell^-$ and $B \to K^*\ell^+\ell^-$*, *Phys. Rev.* **D 73** (2006) 092001 [hep-ex/0604007] [INSPIRE].

JHEP11(2011)121

[14] BABAR collaboration, B. Aubert et al., *Angular Distributions in the Decays $B \to K^* \ell^+ \ell^-$*, *Phys. Rev.* **D 79** (2009) 031102 [arXiv:0804.4412] [INSPIRE].

[15] W. Skiba and J. Kalinowski, *$B_s \to \tau^+ \tau^-$ decay in a two Higgs doublet model*, *Nucl. Phys.* **B 404** (1993) 3.

[16] S. Choudhury and N. Gaur, *Dileptonic decay of B_s meson in SUSY models with large tan β*, *Phys. Lett.* **B 451** (1999) 86 [hep-ph/9810307] [INSPIRE].

[17] C.-S. Huang, W. Liao, Q.-S. Yan and S.-H. Zhu, *$B_s \to \ell^+ \ell^-$ in a general 2 HDM and MSSM*, *Phys. Rev.* **D 63** (2001) 114021 [hep-ph/0006250] [INSPIRE].

[18] C. Bobeth, T. Ewerth, F. Krüger and J. Urban, *Analysis of neutral Higgs boson contributions to the decays $\bar{B}_s \to \ell^+ \ell^-$ and $\bar{B} \to K \ell^+ \ell^-$*, *Phys. Rev.* **D 64** (2001) 074014 [hep-ph/0104284] [INSPIRE].

[19] C.-S. Huang and X.-H. Wu, *$B_s \to \mu^+ \mu^-$ and $B \to X_s \mu^+ mu^-$ in MSSM*, *Nucl. Phys.* **B 657** (2003) 304 [hep-ph/0212220] [INSPIRE].

[20] P.H. Chankowski and L. Slawianowska, *Effects of the scalar FCNC in $b \to s \ell^+ \ell^-$ transitions and supersymmetry*, *Eur. Phys. J.* **C 33** (2004) 123 [hep-ph/0308032] [INSPIRE].

[21] A.K. Alok and S. Sankar, *New physics upper bound on the branching ratio of $B_s \to \ell^+ \ell^-$*, *Phys. Lett.* **B 620** (2005) 61 [hep-ph/0502120] [INSPIRE].

[22] M. Blanke, A.J. Buras, D. Guadagnoli and C. Tarantino, *Minimal Flavor Violation Waiting for Precise Measurements of ΔM_s, $S_{\psi\phi}$, A_{SL}^s, $|V_{ub}|$, γ and $B_{s,d}^0 \to \mu^+ \mu^-$*, *JHEP* **10** (2006) 003 [hep-ph/0604057] [INSPIRE].

[23] A.K. Alok and S.K. Gupta, *$B_s \to \mu^+ \mu^-$ decay in the R-parity violating minimal supergravity*, *Eur. Phys. J.* **C 65** (2010) 491 [arXiv:0904.1878] [INSPIRE].

[24] A.J. Buras, B. Duling, T. Feldmann, T. Heidsieck, C. Promberger and S. Recksiegel, *Patterns of Flavour Violation in the Presence of a Fourth Generation of Quarks and Leptons*, *JHEP* **09** (2010) 106 [arXiv:1002.2126] [INSPIRE].

[25] E. Golowich, J. Hewett, S. Pakvasa, A.A. Petrov and G.K. Yeghiyan, *Relating B_s Mixing and $B_s \to \mu^+ \mu^-$ with New Physics*, *Phys. Rev.* **D 83** (2011) 114017 [arXiv:1102.0009] [INSPIRE].

[26] A. Ali, T. Mannel and T. Morozumi, *Forward backward asymmetry of dilepton angular distribution in the decay $b \to s \ell^+ \ell^-$*, *Phys. Lett.* **B 273** (1991) 505 [INSPIRE].

[27] A.J. Buras and M. Münz, *Effective Hamiltonian for $B \to X_s \ell^+ \ell^-$ beyond leading logarithms in the NDR and HV schemes*, *Phys. Rev.* **D 52** (1995) 186 [hep-ph/9501281] [INSPIRE].

[28] A. Ali, G. Hiller, L. Handoko and T. Morozumi, *Power corrections in the decay rate and distributions in $B \to X_s \ell^+ \ell^-$ in the standard model*, *Phys. Rev.* **D 55** (1997) 4105 [hep-ph/9609449] [INSPIRE].

[29] C.-S. Huang, W. Liao and Q.-S. Yan, *The Promising process to distinguish supersymmetric models with large tan Beta from the standard model: $B \to X_s \mu^+ \mu^-$*, *Phys. Rev.* **D 59** (1999) 011701 [hep-ph/9803460] [INSPIRE].

[30] S. Fukae, C. Kim, T. Morozumi and T. Yoshikawa, *A Model independent analysis of the rare B decay $B \to X_s \ell^+ \ell^-$*, *Phys. Rev.* **D 59** (1999) 074013 [hep-ph/9807254] [INSPIRE].

[31] C. Bobeth, M. Misiak and J. Urban, *Photonic penguins at two loops and m(t) dependence of $BR(B \to X_s \ell^+ \ell^-)$*, *Nucl. Phys.* **B 574** (2000) 291 [hep-ph/9910220] [INSPIRE].

JHEP11(2011)121

[32] A. Ali, E. Lunghi, C. Greub and G. Hiller, *Improved model independent analysis of semileptonic and radiative rare B decays*, *Phys. Rev.* **D 66** (2002) 034002 [hep-ph/0112300] [INSPIRE].

[33] T. Huber, T. Hurth and E. Lunghi, *Logarithmically Enhanced Corrections to the Decay Rate and Forward Backward Asymmetry in $\bar{B} \to X_s \ell^+ \ell^-$*, *Nucl. Phys.* **B 802** (2008) 40 [arXiv:0712.3009] [INSPIRE].

[34] K.S. Lee, Z. Ligeti, I.W. Stewart and F.J. Tackmann, *Extracting short distance information from $b \to s\ell^+\ell^-$ effectively*, *Phys. Rev.* **D 75** (2007) 034016 [hep-ph/0612156] [INSPIRE].

[35] Z. Ligeti and F.J. Tackmann, *Precise predictions for $B \to X_s \ell^+ \ell^-$ in the large q^2 region*, *Phys. Lett.* **B 653** (2007) 404 [arXiv:0707.1694] [INSPIRE].

[36] G. Eilam, C.-D. Lu and D.-X. Zhang, *Radiative dileptonic decays of B mesons*, *Phys. Lett.* **B 391** (1997) 461 [hep-ph/9606444] [INSPIRE].

[37] T. Aliev, A. Ozpineci and M. Savci, *$B_q \to \ell^+\ell^-\gamma$ decays in light cone QCD*, *Phys. Rev.* **D 55** (1997) 7059 [hep-ph/9611393] [INSPIRE].

[38] C. Geng, C. Lih and W.-M. Zhang, *Study of $B_{s,d} \to \ell^+\ell^-\gamma$ decays*, *Phys. Rev.* **D 62** (2000) 074017 [hep-ph/0007252] [INSPIRE].

[39] Y. Dincer and L.M. Sehgal, *Charge asymmetry and photon energy spectrum in the decay $B_s \to \ell^+\ell^-\gamma$*, *Phys. Lett.* **B 521** (2001) 7 [hep-ph/0108144] [INSPIRE].

[40] F. Krüger and D. Melikhov, *Gauge invariance and form-factors for the decay $B \to \gamma\ell^+\ell^-$*, *Phys. Rev.* **D 67** (2003) 034002 [hep-ph/0208256] [INSPIRE].

[41] D. Melikhov and N. Nikitin, *Rare radiative leptonic decays $B_{d,s} \to \ell^+\ell^-\gamma$*, *Phys. Rev.* **D 70** (2004) 114028 [hep-ph/0410146] [INSPIRE].

[42] D. Melikhov, N. Nikitin and K. Toms, *Rare radiative leptonic decays $B_{d,s} \to \ell^+\ell^-\gamma$*, *Phys. Atom. Nucl.* **68** (2005) 1842 [INSPIRE].

[43] A.K. Alok and S. Uma Sankar, *New physics upper bound on the branching ratio of $B_s \to \ell^+\ell^-\gamma$*, *Mod. Phys. Lett.* **A 22** (2007) 1319 [hep-ph/0603262] [INSPIRE].

[44] I. Balakireva, D. Melikhov, N. Nikitin and D. Tlisov, *Forward-backward and CP-violating asymmetries in rare $B_{d,s} \to (V,\gamma)\ell^+\ell^-$ decays*, *Phys. Rev.* **D 81** (2010) 054024 [arXiv:0911.0605] [INSPIRE].

[45] A. Ali, P. Ball, L. Handoko and G. Hiller, *A Comparative study of the decays $B \to (K, K^*)\ell^+\ell^-$ in standard model and supersymmetric theories*, *Phys. Rev.* **D 61** (2000) 074024 [hep-ph/9910221] [INSPIRE].

[46] T. Aliev, M. Cakmak, A. Ozpineci and M. Savci, *New physics effects to the lepton polarizations in the $B \to K\ell^+\ell^-$ decay*, *Phys. Rev.* **D 64** (2001) 055007 [hep-ph/0103039] [INSPIRE].

[47] W. Bensalem, D. London, N. Sinha and R. Sinha, *Lepton polarization and forward backward asymmetries in $b \to s\tau^+\tau^-$*, *Phys. Rev.* **D 67** (2003) 034007 [hep-ph/0209228] [INSPIRE].

[48] C. Bobeth, G. Hiller and G. Piranishvili, *Angular distributions of $B \to K\ell\ell$ decays*, *JHEP* **12** (2007) 040 [arXiv:0709.4174] [INSPIRE].

[49] A.K. Alok, A. Dighe and S. Uma Sankar, *Large forward-backward asymmetry in $B \to K\mu^+\mu^-$ from new physics tensor operators*, *Phys. Rev.* **D 78** (2008) 114025 [arXiv:0810.3779] [INSPIRE].

JHEP11(2011)121

[50] J. Charles, A. Le Yaouanc, L. Oliver, O. Pene and J. Raynal, *Heavy to light form-factors in the heavy mass to large energy limit of QCD*, *Phys. Rev.* **D 60** (1999) 014001 [hep-ph/9812358] [INSPIRE].

[51] M. Beneke and T. Feldmann, *Symmetry breaking corrections to heavy-to-light B meson form-factors at large recoil*, *Nucl. Phys.* **B 592** (2001) 3 [hep-ph/0008255] [INSPIRE].

[52] F. Krüger and E. Lunghi, *Looking for novel CP-violating effects in $\bar{B} \to K^* \ell^+ \ell^-$*, *Phys. Rev.* **D 63** (2001) 014013 [hep-ph/0008210] [INSPIRE].

[53] M. Beneke, T. Feldmann and D. Seidel, *Systematic approach to exclusive $B \to V \ell^+ \ell^-, V\gamma$ decays*, *Nucl. Phys.* **B 612** (2001) 25 [hep-ph/0106067] [INSPIRE].

[54] Q.-S. Yan, C.-S. Huang, W. Liao and S.-H. Zhu, *Exclusive semileptonic rare decays $B \to (K, K^*)\ell^+\ell^-$ in supersymmetric theories*, *Phys. Rev.* **D 62** (2000) 094023 [hep-ph/0004262] [INSPIRE].

[55] T. Aliev, V. Bashiry and M. Savci, *Double lepton polarization asymmetries in the $B \to K \ell^+ \ell^-$ decay beyond the standard model*, *Eur. Phys. J.* **C 35** (2004) 197 [hep-ph/0311294] [INSPIRE].

[56] T. Aliev, V. Bashiry and M. Savci, *Polarized lepton pair forward backward asymmetries in $B \to K^* \ell^+ \ell^-$ decay beyond the standard model*, *JHEP* **05** (2004) 037 [hep-ph/0403282] [INSPIRE].

[57] F. Krüger and J. Matias, *Probing new physics via the transverse amplitudes of $B^0 \to K^{*0}(\to K^-\pi^+)\ell^+\ell^-$ at large recoil*, *Phys. Rev.* **D 71** (2005) 094009 [hep-ph/0502060] [INSPIRE].

[58] E. Lunghi and J. Matias, *Huge right-handed current effects in $B \to K^*(K\pi)\ell^+\ell^-$ in supersymmetry*, *JHEP* **04** (2007) 058 [hep-ph/0612166] [INSPIRE].

[59] A. Hovhannisyan, W.-S. Hou and N. Mahajan, *$B \to K^* \ell^+ \ell^-$ Forward-backward Asymmetry and New Physics*, *Phys. Rev.* **D 77** (2008) 014016 [hep-ph/0701046] [INSPIRE].

[60] U. Egede, T. Hurth, J. Matias, M. Ramon and W. Reece, *New observables in the decay mode $\bar{B} \to \bar{K}^{*0} \ell^+ \ell^-$*, *JHEP* **11** (2008) 032 [arXiv:0807.2589] [INSPIRE].

[61] W. Altmannshofer, P. Ball, A. Bharucha, A.J. Buras, D.M. Straub and M. Wick, *Symmetries and Asymmetries of $B \to K^* \mu^+ \mu^-$ Decays in the Standard Model and Beyond*, *JHEP* **01** (2009) 019 [arXiv:0811.1214] [INSPIRE].

[62] A.K. Alok et al., *New-physics contributions to the forward-backward asymmetry in $B \to K^* \mu^+ \mu^-$*, *JHEP* **02** (2010) 053 [arXiv:0912.1382] [INSPIRE].

[63] A. Soni, A.K. Alok, A. Giri, R. Mohanta and S. Nandi, *SM with four generations: Selected implications for rare B and K decays*, *Phys. Rev.* **D 82** (2010) 033009 [arXiv:1002.0595] [INSPIRE].

[64] C. Bobeth, G. Hiller and D. van Dyk, *The Benefits of $\bar{B} \to \bar{K}^* \ell^+ \ell^-$ Decays at Low Recoil*, *JHEP* **07** (2010) 098 [arXiv:1006.5013] [INSPIRE].

[65] E. Lunghi and A. Soni, *An improved observable for the forward-backward asymmetry in $B \to K^* \ell^+ \ell^-$ and $B_s \to \phi \ell^+ \ell^-$*, *JHEP* **11** (2010) 121 [arXiv:1007.4015] [INSPIRE].

[66] C. Bobeth, G. Hiller and D. van Dyk, *More Benefits of Semileptonic Rare B Decays at Low Recoil: CP-violation*, *JHEP* **07** (2011) 067 [arXiv:1105.0376] [INSPIRE].

JHEP11(2011)121

[67] A. Bharucha and W. Reece, *Constraining new physics with $B \to K^* \mu^+ \mu^-$ in the early LHC era*, *Eur. Phys. J.* **C 69** (2010) 623 [arXiv:1002.4310] [INSPIRE].

[68] G. Hiller and F. Krüger, *More model independent analysis of $b \to s$ processes*, *Phys. Rev.* **D 69** (2004) 074020 [hep-ph/0310219] [INSPIRE].

[69] A.K. Alok, A. Dighe and S. Sankar, *Tension between scalar/pseudoscalar new physics contribution to $B_s \to \mu^+ \mu^-$ and $B \to K \mu^+ \mu^-$*, *Mod. Phys. Lett.* **A 25** (2010) 1099 [arXiv:0803.3511] [INSPIRE].

[70] A.K. Alok, A. Dighe and S. Sankar, *Probing extended Higgs sector through rare $b \to s \mu^+ \mu^-$ transitions*, *Phys. Rev.* **D 78** (2008) 034020 [arXiv:0805.0354] [INSPIRE].

[71] M. Beylich, G. Buchalla and T. Feldmann, *Theory of $B \to K^* \ell^+ \ell^-$ decays at high q^2: OPE and quark-hadron duality*, *Eur. Phys. J.* **C 71** (2011) 1635 [arXiv:1101.5118] [INSPIRE].

[72] A.K. Alok, A. Datta, A. Dighe, M. Duraisamy, D. Ghosh, et al., *New Physics in $b \to s \mu^+ \mu^-$: CP-Violating Observables*, arXiv:1103.5344 [INSPIRE].

[73] B. Grinstein and D. Pirjol, *Symmetry breaking corrections to heavy meson form-factor relations*, *Phys. Lett.* **B 533** (2002) 8 [hep-ph/0201298] [INSPIRE].

[74] B. Grinstein and D. Pirjol, *Exclusive rare $B \to K^* \ell^+ \ell^-$ decays at low recoil: Controlling the long-distance effects*, *Phys. Rev.* **D 70** (2004) 114005 [hep-ph/0404250] [INSPIRE].

[75] P. Gambino, U. Haisch and M. Misiak, *Determining the sign of the $b \to s \gamma$ amplitude*, *Phys. Rev. Lett.* **94** (2005) 061803 [hep-ph/0410155] [INSPIRE].

[76] CDF collaboration, T. Aaltonen et al., *Search for $B_s^0 \to \mu^+ \mu^-$ and $B_d^0 \to \mu^+ \mu^-$ decays with $2 f b^{-1}$ of $p \bar{p}$ collisions*, *Phys. Rev. Lett.* **100** (2008) 101802 [arXiv:0712.1708] [INSPIRE].

[77] PARTICLE DATA GROUP collaboration, C. Amsler et al., *Review of Particle Physics*, *Phys. Lett.* **B 667** (2008) 1 [INSPIRE].

[78] HEAVY FLAVOR AVERAGING GROUP collaboration, E. Barberio et al., *Averages of $b-$hadron and $c-$hadron Properties at the End of 2007*, arXiv:0808.1297 [INSPIRE].

[79] BABAR collaboration, B. Aubert et al., *Measurement of the $B \to X_s \ell^+ \ell^-$ branching fraction with a sum over exclusive modes*, *Phys. Rev. Lett.* **93** (2004) 081802 [hep-ex/0404006] [INSPIRE].

[80] BELLE collaboration, M. Iwasaki et al., *Improved measurement of the electroweak penguin process $B \to X_s \ell^+ \ell^-$*, *Phys. Rev.* **D 72** (2005) 092005 [hep-ex/0503044] [INSPIRE].

[81] J. Laiho, E. Lunghi and R.S. Van de Water, *Lattice QCD inputs to the CKM unitarity triangle analysis*, *Phys. Rev.* **D 81** (2010) 034503 [arXiv:0910.2928] [INSPIRE].

[82] M. Lenzi, *Rare B decays at LHCb*, arXiv:0710.5056 [INSPIRE].

[83] T.E. Browder, T. Gershon, D. Pirjol, A. Soni and J. Zupan, *New Physics at a Super Flavor Factory*, *Rev. Mod. Phys.* **81** (2009) 1887 [arXiv:0802.3201] [INSPIRE].

[84] BABAR collaboration, B. Aubert et al., *Measurements of branching fractions, rate asymmetries and angular distributions in the rare decays $B \to K \ell^+ \ell^-$ and $B \to K^* \ell^+ \ell^-$*, *Phys. Rev.* **D 73** (2006) 092001 [hep-ex/0604007] [INSPIRE].

[85] BELLE COLLABORATION collaboration, K. Ikado, *Measurements of forward-backward asymmetry in $B \to K^* \ell^+ \ell^-$ and evidence of $B^- \to \tau^- \bar{\nu}$*, hep-ex/0605067 [INSPIRE].

JHEP11(2011)121

[86] ATLAS and CMS collaborations, C. Adorisio, *Studies of Semileptonic Rare B Decays at ATLAS and CMS*, talk given at CERN Theory Institute, CERN, Geneva Switzerland, May 2008, http://indico.cern.ch/conferenceOtherViews.py?view=standard&confId=31959.

[87] The LHCb collaboration, B. Adeva et al., *Roadmap for selected key measurements of LHCb*, arXiv:0912.4179 [INSPIRE].

[88] C.-H. Chen and C. Geng, *Analysis of $B \to K^* \ell^+ \ell^-$ decays at large recoil region*, *Nucl. Phys.* **B 636** (2002) 338 [hep-ph/0203003] [INSPIRE].

[89] C.-H. Chen and C. Geng, *Probing new physics in $B \to K^* \ell^+ \ell^-$ decays*, *Phys. Rev.* **D 66** (2002) 094018 [hep-ph/0209352] [INSPIRE].

[90] CDF collaboration, T. Aaltonen et al., *Search for $B_s \to \mu^+ \mu^-$ and $B_d \to \mu^+ \mu^-$ Decays with CDF II*, *Phys. Rev. Lett.* **107** (2011) 191801 [arXiv:1107.2304] [INSPIRE].

[91] J. Serrano, *The search for the very rare decays $B_{(s,d)} \to \mu^+ \mu^-$ at LHCb*, talk at *Europhysics Conference on High-Energy Physics (EPS-HEP 2011)*, Grenoble France, July 2011.

[92] M. Patel, *Angular analysis of the decay $Bd \to K^* \mu\mu$ at LHCb*, talk at *Europhysics Conference on High-Energy Physics (EPS-HEP 2011)*, Grenoble France, July 2011.

[93] CKMfitter Group collaboration, J. Charles et al., *CP violation and the CKM matrix: Assessing the impact of the asymmetric B factories*, *Eur. Phys. J.* **C 41** (2005) 1 [hep-ph/0406184] [INSPIRE].

JHEP11(2011)121